AD NUMBER

ADB004278

LIMITATION CHANGES

TO:

Approved for public release; distribution is unlimited.

FROM:

Distribution authorized to U.S. Gov't. agencies only; Test and Evaluation; MAY 1975. Other requests shall be referred to Air Force Avionics Lab., Wright-Patterson AFB, OH 45433.

AUTHORITY

AFAL ltr 12 Sep 1977

AFAL-TR-75-66

MICRO-NAVIGATOR (MICRON) ANALYSIS

SIMULATION AND TEST SUPPORT STUDIES

James D. Shields

THE ANALYTIC SCIENCES CORPORATION

Technical Report AFAL-TR-75-66

May 1975

Air Force Avionics Laboratory
Air Force Systems Command
Wright-Patterson Air Force Base
Ohio 45433

NOTICE

When Government drawings, specifications, or other data are used for any purpose other than in connection with a definitely related Government procurement operation, the United States Government thereby incurs no responsibility nor any obligation whatsoever; and the fact that the government may have formulated, furnished, or in any way supplied the said drawings, specifications, or other data, is not to be regarded by implication or otherwise as in any manner licensing the holder or any other person or corporation, or conveying any rights or permission to manufacture, use, or sell any patented invention that may in any way be related thereto.

Copies of this report should not be returned unless return is required by security considerations, contractual obligations, or notice on a specific document.

Unclassified

SECURITY CLASSIFICATION DF THIS PAGE (When Data Entered)

REPORT DOCUMENTATION PAGE		READ INSTRUCTIONS BEFORE COMPLETING FORM
1. REPORT NUMBER AFAL-TR-75-66	2. GDVT ACCESSION NO.	3. RECIPIENT'S CATALDG NUMBER
4. TITLE (and Subtitle) MICRO-NAVIGATOR (MICRON) ANALYSIS Simulation and Test Support Studies		5. TYPE OF REPORT & PERIOD COVERED Final Report October 1972-May 1974
		6. PERFORMING ORG. REPORT NUMBER TR-316-3-2
7. AUTHOR(s) James D. Shields		8. CONTRACT OR GRANT NUMBER(s) F33615-72-C-1787
9. PERFORMING ORGANIZATION NAME AND ADDRESS The Analytic Sciences Corporation 6 Jacob Way Reading, Massachusetts 01867		10. PROGRAM ELEMENT, PRDJECT, TASK AREA & WORK UNIT NUMBERS Advanced Development Program 666A, Task Number 02
11. CONTRDLLING DFFICE NAME AND ADDRESS Air Force Avionics Laboratory (RWM/666A) Air Force Systems Command Wright-Patterson AFB, Ohio 45433		12. REPDRT DATE May 1975 13. NUMBER DF PAGES 102
14. MONITDRING AGENCY NAME & ADDRESS(if different from Controlling Office)		15. SECURITY CLASS. (of this report) Unclassified 15a. DECLASSIFICATION/DOWNGRADING SCHEDULE

16. DISTRIBUTION STATEMENT (of this Report)

Distribution limited to U.S. Government agencies only, Test and Evaluation, May 1975. Other requests for this document must be referred to AFAL (RWM/666A), Wright-Patterson AFB, Ohio 45433.

17. DISTRIBUTIDN STATEMENT (of the abstract entered in Block 20, if different from Report)

18. SUPPLEMENTARY NOTES

19. KEY WDRDS (Continue on reverse side if necessary and identify by block number)

MICRON
Inertial Navigation Error Analysis
Inertial System Simulation
INS Testing

20. ABSTRACT (Continue on reverse side if necessary and identify by block number)

Results in three areas of MICRON system level analysis are presented. The MICRON Computer Simulation Program (MCSP) which directly simulates the system mechanization equations is used to investigate system performance during several proposed MESG instrument variations and during severe environments. Equations describing the propagation of instrument errors into MICRON navigation errors are derived and coded into a covariance

DD FORM 1 JAN 73 1473 EDITION OF 1 NOV 65 IS OBSOLETE

Unclassified

SECURITY CLASSIFICATION DF THIS PAGE (When Data Entered)

20. ABSTRACT (Continued)

analysis computer program for use in statistical performance analysis studies. The covariance analysis program is used to determine the propagation characteristics of those error sources which are unique to the MICRON system. Activities in support of the test program for the N57A demonstration system are described. These activities include critical review of the Test Plan and evaluation of the test data.

TABLE OF CONTENTS

LIST OF FIGURES

LIST OF TABLES

1. INTRODUCTION

1.1 OVERVIEW

A strapdown micro-navigator (MICRON) is presently under development by AFAL/Autonetics for applications requiring a small, reliable, moderately accurate inertial navigator. The entire set of inertial sensors in MICRON consists of two Micro-Electrostatic Gyro Accelerometers (MESGA's). As part of the development of MICRON, a strapdown inertial navigator designated as N57A is being fabricated and tested (Ref. 6). This system uses three accelerometers for measuring specific force and two Micro-Electrostatic Gyros (MESG's) for maintaining an inertial reference. The physical characteristics of the MESG are identical to those of the MESGA. The N57A is intended to demonstrate MICRON's function and performance, but not MICRON's ultimate small size.

TASC has been performing analytic studies in support of the MICRON development program since March 1971 through a sequence of contracts with AFAL. Previous investigations have looked chiefly at the MESG instrument, developing models to describe the MESG drift rate and attitude readout (ARO) errors (Refs. 1, 2, and 3) and evaluating UNICAL, a procedure proposed by TASC to simultaneously calibrate both the drift rate and ARO error models (Refs. 3 and 4). This report documents a set of system level analyses that have been conducted to support the development of MICRON. These analyses were conducted in three areas: direct simulation of MICRON system performance using the MICRON Computer Simulation Program (MCSP), derivation of error analysis equations and

development of a computer program implementing these to conduct statistical performance studies, and support of the N57A test program.

The MCSP, which simulates directly the mechanization equations that are implemented in MICRON (see Fig. 1.1-1), was developed during previous MICRON studies and is described in detail in Ref. 3. The MCSP was used to investigate the navigation performance of the MICRON system during four different cases:

- Reduced preload charge levels on the MESG.
- Severe vibration environment.
- High vehicle roll rates and accelerations
- Instrument errors due solely to miscalibration (i.e., assuming no errors due to turn-on-to-turn-on repeatability).

Plots of the navigation errors occurring in each of these cases were generated.

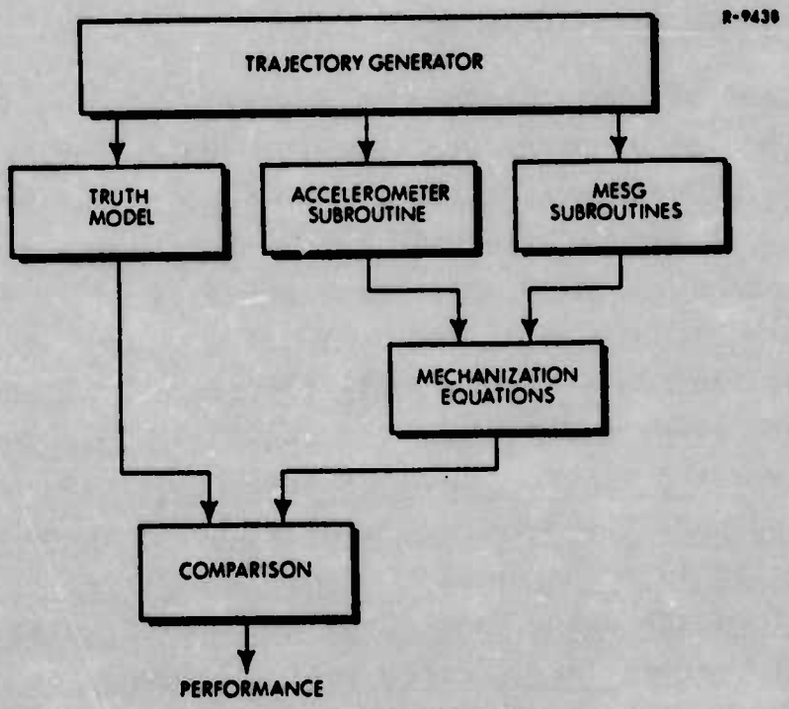

Figure 1.1-1 MCSP Flow Diagram

To complement the MCSP and to enhance the total capability to simulate MICRON performance, a covariance error analysis computer program was developed. The covariance error analysis technique allows the generation of the statistics describing MICRON's navigation performance for an ensemble of trials over the same trajectory in a single computer run. (To conduct statistical performance studies with the deterministic MCSP would require costly Monte Carlo analysis.) This report derives the MICRON error equations, which model the propagation of instrument errors into system navigation errors, and describes the implementation of these equations in the error analysis computer program. The results of a study to investigate the error propagation characteristics of those error sources that are unique to MICRON are also presented.

The final activity discussed in this document is the TASC support of the N57A test program. The Test Plan developed by Autonetics (Ref. 20) is reviewed and recommended improvements are suggested. The results of the laboratory and van tests on the N57A system are evaluated and the system performance is compared with the specified performance values (Ref. 5).

1.2 OUTLINE OF THE REPORT

Chapter 2 presents the results of the MCSP studies. Section 2.1 briefly describes the MCSP while Sections 2.2, 2.3, and 2.4 present the simulated MICRON navigation performance for the four cases that were investigated. A brief overview of the mechanization equations is presented in Section 3.1 while the error equations which describe the MICRON system are derived in Section 3.2. Section 3.3 discusses the

error analysis computer program and presents the results that were generated with it. The N57A Test Plan is reviewed in Section 4.1, and the results of the test program are discussed in Section 4.2.

2. MICRON COMPUTER SIMULATION PROGRAM (MCSP) STUDIES

The MICRON Computer Simulation Program (MCSP), described in Ref. 3, was used to investigate the effects of severe environments and of several proposed MESG variations on MICRON navigation performance. The environmental studies consisted of determining the performance degradation induced by vibration inputs and by high vehicle roll rates. The MESG variation studies evaluated the predicted navigation performance for cases when the gyro preload charge level was reduced and when there were no gyro repeatability errors (i.e., the only MESG errors were due to the calibration procedure).

A brief description of the MCSP is presented in Section 2.1. The results of the MESG variation studies are given in Section 2.2, while the vibration and high roll rate results are presented in Sections 2.3 and 2.4, respectively.

2.1 MCSP DESCRIPTION

The MICRON Computer Simulation Program (MCSP) is a flexible research tool for investigating the performance of the MICRON system. The program is a direct, deterministic simulation which allows study of the parametric behavior of the MICRON system, its hardware and its software, under a variety of dynamic conditions. The MCSP is a direct simulation since it duplicates the mechanization equations used in the N57A (a developmental system, using three

accelerometers to measure specific force and two MESG's to maintain an attitude reference, which demonstrated MICRON's function and performance, but not its ultimate small size). It is a deterministic simulation since the program input parameters describing the system error sources are "sample inputs;" and, the simulation results generated by the MCSP are the "sample outputs" corresponding to these inputs. To perform a statistical analysis of predicted MICRON navigation performance using the MCSP, it would be necessary to make a large number of simulation runs drawing the input parameters from appropriate distributions and average the entire ensemble of results that were generated (i.e., to perform Monte Carlo analysis).

The MCSP, diagrammed in Fig. 1.1-1, has been developed in a modular form to facilitate modifications and additions as the MICRON system design is altered or new areas require investigation. The principal program modules include a trajectory generator/truth model (TG/TM), several subroutines which model the inertial instruments, and a module that duplicates the system mechanization equations. The TG/TM supplies a dynamic motion environment with which to exercise the MCSP and includes an accurate model of position and velocity against which to evaluate the MICRON computation of these quantities. The TG/TM allows the selection of several different trajectories (see Ref. 3) for use in MICRON evaluation.

Incorporated into the MCSP is a detailed simulation of the Micro-Electrostatic Gyro (MESG) which includes the prominent drift rate and attitude readout (ARO) error mechanisms. As described in detail in Ref. 3, only residual (those which remain following compensation) MESG errors are used in the MCSP. This procedure simplifies the simulation program by eliminating the necessity of implementing the full

MESG compensation formulas. Parameters descriptive of the MESG residual errors for the case to be studied are part of the MCSP input data. For the current studies, the accelerometers have been modeled as ideal instruments.

The execution rate of the MCSP is set by three parameters: fast loop frequency (FLF), slow loop frequency (SLF), and truth loop frequency (TLF). The first two are MICRON system parameters which indicate how often the inertial sensors are sampled and how often the navigation equations are solved. For the MICRON system these are 64 and 16 times per second, respectively. The truth loop frequency indicates how often the navigation reference quantities (i.e., true position, velocity, and attitude) are updated by the trajectory generator. All three iteration rates may be varied independently in the MCSP. This desirable feature provides the capability to investigate different solution rates for the mechanization equations and to vary the truth loop frequency as a function of the trajectory allowing efficient, yet accurate, reference computations for dynamic environments of varying frequency content.

Because it duplicates the MICRON mechanization and consequently requires a large amount of computer time to execute, the MCSP is most useful for studies which can be conducted using short duration trajectories and which require the level of detail which the MCSP offers. Most long-term navigation performance investigations do not require the detail of a direct simulation. For these studies, a covariance error analysis program, which allows a statistical characterization of the system performance, is a more appropriate analytic tool. The preliminary development of a covariance error analysis program for MICRON is described in Chapter 3.

2.2 MESG VARIATION STUDIES

The MESG variation studies investigated the effect on MICRON navigation accuracy of four different levels of MESG errors. These residual error levels represent the errors for various operational or design variations potentially available to the MICRON system designers. For each case, the MCSP input parameters that model the MESG were varied to yield the appropriate residual drift rate and ARO errors, and the simulation program was exercised to determine the resulting navigation errors. Table 2.2-1 presents the residual values that were used in these studies to represent:

- Perfect MESG's (i.e., no drift rate or ARO error).
- Nominal MESG's
- MESG's with errors due only to miscalibration
- MESG's with the preload charge level reduced by 30%

The values chosen to describe the drift rate and ARO error residuals were based on the MICRON performance specifications and on data collected by Autonetics during MESG testing.

TABLE 2.2-1

RESIDUAL ERRORS FOR MESG VARIATION STUDIES

MESG VARIATIONS	RESIDUAL DRIFT RATE (deg/hr)	RESIDUAL ARO ERROR (mrad)
Perfect MESG's	0.0	0.0
Nominal MESG's	0.0100	0.100
MESG's with only calibration errors	0.0092	0.078
Reduced Preload MESG's	0.0070	0.110

The residual error levels selected for the nominal MESG and for the MESG which exhibited calibration errors only are the targets called out in the MICRON specification (Ref. 5). Since Autonetics has demonstrated (Ref. 6) that these target MESG error residuals are attainable, their use in this performance evaluation study is reasonable. MESG reduced preload studies conducted by Autonetics (Refs. 7 and 8) indicated that using a preload charge level equal to 70% of the nominal value leads to a 30% reduction in drift rate residuals and a 10% increase in residual ARO errors.

Figure 2.2-1 presents the trajectory which was used for the MESG variation studies. The aircraft speed for this 5 min, constant altitude (24,000 ft) trajectory is 600 ft/sec. During the turn, the heading rate is 0.75 deg/sec. Since the MICRON alignment procedure was not investigated in these studies, the navigation initial position, velocity and attitude errors were set to zero. A more detailed description of this trajectory is presented with the MCSP development in Ref. 3.

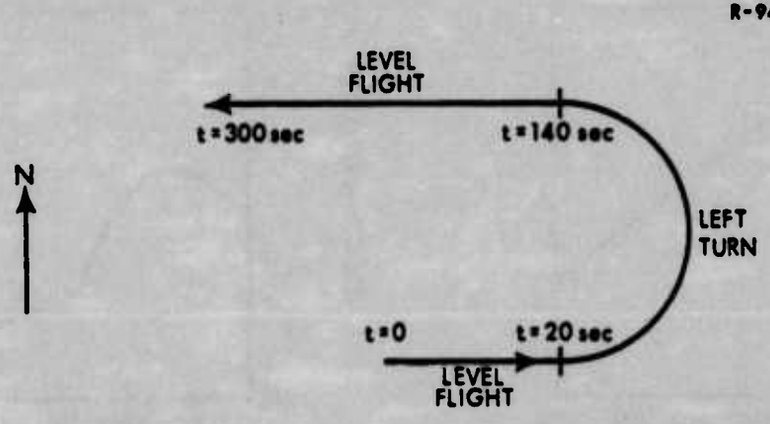

Figure 2.2-1 Trajectory for MESG Variation Studies

The time histories of the MICRON navigation errors for the MCSP run using nominal MESG error levels are presented in Fig. 2.2-2. Examination of these results indicates that the turn in the trajectory induces a MICRON

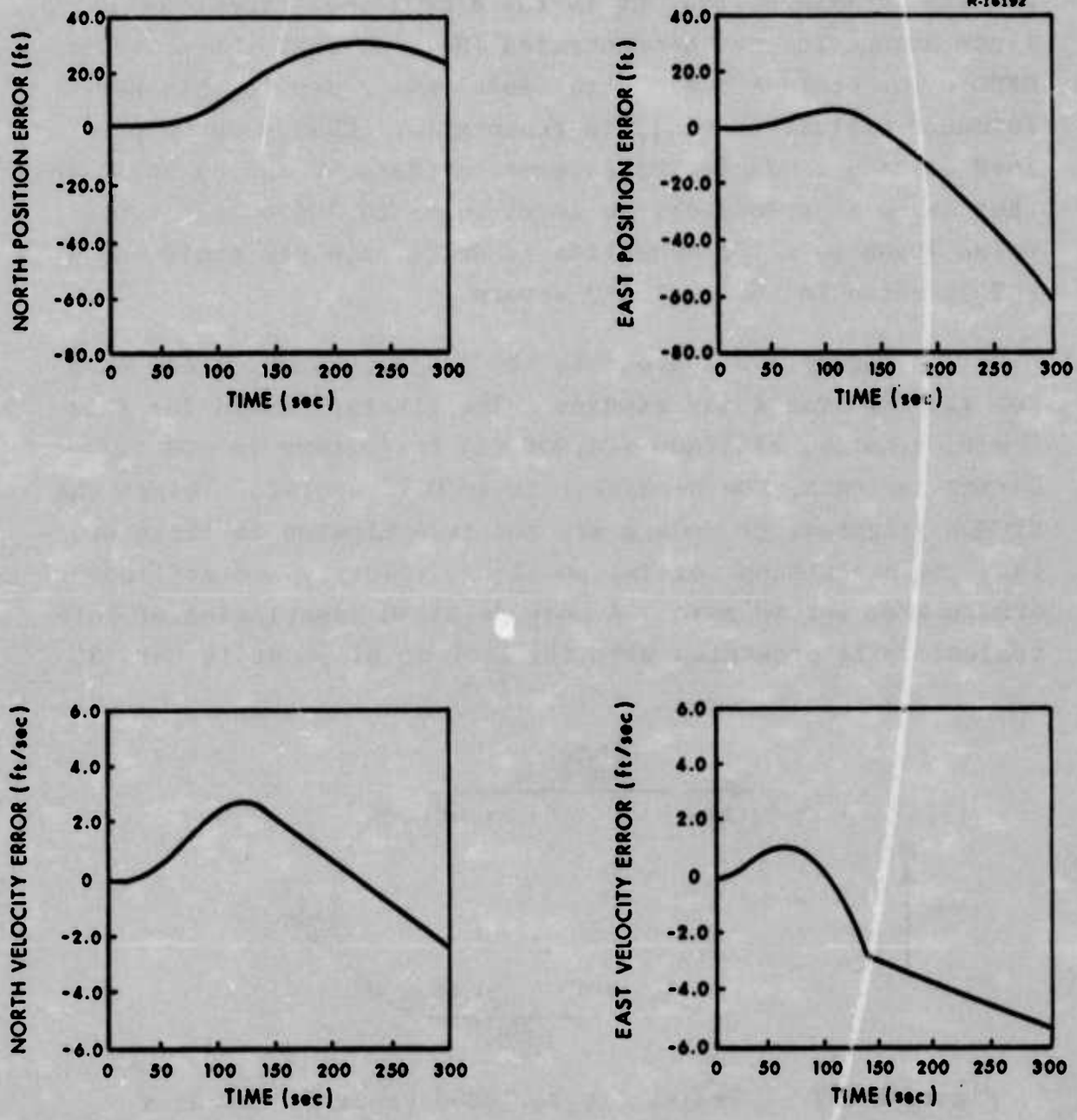

Figure 2.2-2 Single Trial Monte Carlo MICRON System Performance With Nominal MESG Errors

velocity error. This error results from misresolution of sensed acceleration due to ARO errors and misalignments between the true navigation frame and the computational frame caused by drift of the MESG's (see Ref. 9 for a discussion of error propagation in inertial navigation systems). At the completion of the turn when the aircraft acceleration is zero, the velocity error behavior will exhibit the classical 84-min period Schuler oscillation, although the trajectory is too short to clearly demonstrate this behavior.

The navigation errors for each of the four cases investigated in the MESG variation study have similar trajectory-induced time histories to those presented in Fig. 2.2-2 for the nominal MESG errors. The magnitudes of these errors vary indicating the navigation performance attainable with each of the four levels of MESG errors. Table 2.2-2 presents the terminal navigation errors for the 5-min trajectory diagrammed in Fig. 2.2-1. The errors for the perfect MESG run indicate the navigation errors due solely to mechanization of the MICRON navigation equations (iteration rates, integration algorithms, etc.). Table 2.2-2 shows that mechanization errors do not dominate MICRON performance for this trajectory since they account for less than 10% of the navigation error when nominal error levels are used to describe the MESG.

It is important to note that the results presented in Table 2.2-2 are single trial Monte Carlo runs (one set of sample inputs producing a single set of sample outputs) and as with single samples of a random process, care must be exercised when interpreting the results. (Table 2.2-2 does not present statistical performance predictions for the proposed MICRON configurations.) In generating the results presented in Table 2.2-2, it was assumed that the trajectory was preceded by a perfect alignment; and consequently, the

TABLE 2.2-2

SINGLE TRIAL MONTE CARLO TERMINAL NAVIGATION ERRORS FOR MESG VARIATION STUDY

MESG VARIATION	NORTH POSITION ERROR (ft)	EAST POSITION ERROR (ft)	RADIAL POSITION ERROR (ft)	NORTH VELOCITY ERROR (ft/sec)	EAST VELOCITY ERROR (ft/sec)	RADIAL VELOCITY ERROR (ft/sec)
Perfect MESG's	- 2.1	- 3.8	4.3	-0.010	-0.034	0.054
Nominal MESG's	20.8	-60.3	63.8	-0.226	-0.525	0.571
MESG's with calibration errors only	14.4	-54.1	56.0	-0.228	-0.412	0.471
Reduced Preload MESG's	27.7	-48.7	56.0	-0.105	-0.477	0.488

terminal errors are smaller than would be expected from the actual MICRON system since the propagation of initial alignment errors into system performance errors has not been included. For these reasons, the conclusions developed from the results presented in Table 2.2-2 will be based on the relative performance of the various configurations rather than on the absolute performance data generated.

The study indicates that performance improvement of about 15% is attained either by reducing the preload charge level by 30% or by reducing the MESG errors to the level specified for calibration accuracy (thus not including errors due to repeatability of calibration coefficients across a shutdown). Although the simulation results indicate that better navigation performance can be attained by reducing the preload charge level, this change was not incorporated into the MICRON system since the maximum suspension force that can be generated by the MESG would be too small. The suspension force is related to the square of the charge level; consequently, reducing the preload charge by 30% reduces the maximum suspension force by approximately 50%.

Reducing the total residual MESG errors to the levels specified for calibration accuracy is an available design option achievable by improving total instrument performance and/or improving the MESG error compensation parameter stability across a power cycle. These studies present the performance improvement which can be expected from this change. The expected performance gain must be traded against the other MICRON targets (cost, reliability, etc.) prior to reaching a design decision.

2.3 VIBRATION STUDIES

The MCSP was also used to investigate the sensitivity of navigation accuracy to correlated linear and angular vibrations. As shown in Fig. 2.3-1, the vibro-pendulous motion that was used for this study could be generated by mounting the MICRON system on the end of a pendulum. The three parameters which characterize this motion are: LMA, the length of the moment arm; β_{max}, the maximum angular displacement, and ω_p, the frequency of the vibration. A detailed description of the vibro-pendulous motion trajectory is presented in Ref. 3.

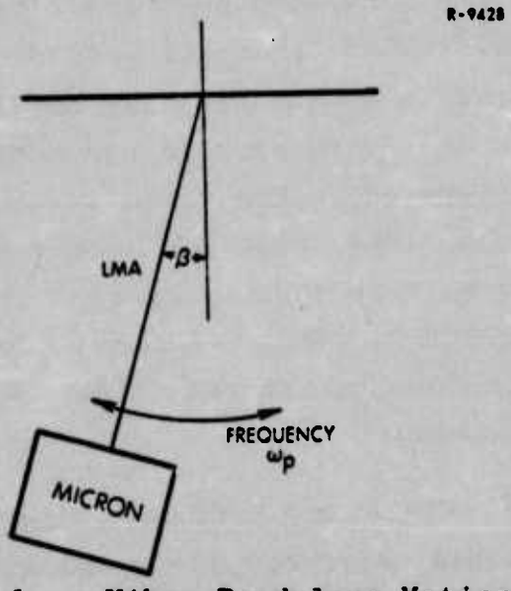

Figure 2.3-1 Vibro-Pendulous Motion Model for MCSP Vibration Studies

It can be shown that the maximum acceleration normal to the moment arm on a body under the vibro-pendulous motion described in Fig. 2.3-1 is

$$a_{n_{max}} = LMA\ \omega_p^2\ \beta_{max} \qquad (2.3\text{-}1)$$

For these studies, the maximum angular displacement was defined in terms of the vibration frequency as

$$\beta_{max} = \frac{k}{\omega_p^2} \qquad (2.3\text{-}2)$$

where $k = 1\ sec^{-2}$. Because of the definition in Eq. (2.3-2), the maximum normal acceleration can be varied independently of the frequency of vibration by changing the value of LMA.

The vibration environment studies were principally concerned with the sensitivity of the navigation accuracy to input frequencies close to the fast and slow loop frequencies of the MICRON mechanization. The fast loop operations which consist of sampling the inertial sensors occur at 64 times per second while the slow loop solution of the navigation equations is completed 16 times per second. Table 2.3-1 presents the vibration frequencies and maximum normal acceleration levels that were used in the MCSP vibration studies. Also presented in the table is the value of the truth loop frequency (TLF) used for each run. As described in Ref. 3, TLF is an MCSP input parameter that controls the frequency of solution of the truth model equations generating the reference values against which the MICRON navigation outputs are compared.

Figures 2.3-2 and 2.3-3 present single-trial navigation error time histories for 30-second MCSP runs for

TABLE 2.3-1

VIBRATION FREQUENCIES AND NORMAL ACCELERATIONS FOR MCSP VIBRATION STUDIES

CASE	VIBRATION FREQUENCY (Hz)	MAX a_n (g's)	TLF
Baseline	0	0	64
1	120	0.10	256
2	120	0.03	256
3	90	0.10	256
4	90	0.03	256
5	60	0.10	128
6	60	0.03	128
7	20	3.00	64
8	5	2.00	64

the baseline and Case 1, respectively. For all the vibration studies, the nominal residual error parameters were used to describe the MESG's. As illustrated by Fig. 2.3-3, the vibro-pendulous environment causes oscillatory velocity errors. Because of the oscillatory nature of the velocity errors in the vibration environment, Table 2.3-2 (which summarizes the results of the MCSP vibration studies) presents the maximum errors during the 30 seconds of vibration rather than the terminal navigation errors.

The results of the MCSP vibration studies indicate that vibro-pendulous input motion does not cause any unacceptable navigation errors. The errors caused by the low amplitude, high frequency vibrations are quite small relative to MICRON's performance specifications of 1 nm/hr position error growth rate and 5 ft/sec velocity error. The lower frequency, high g-level vibrations generated sizable navigation errors. Reference 10 presents a plot of the vibration amplitude as a function of the frequency to which

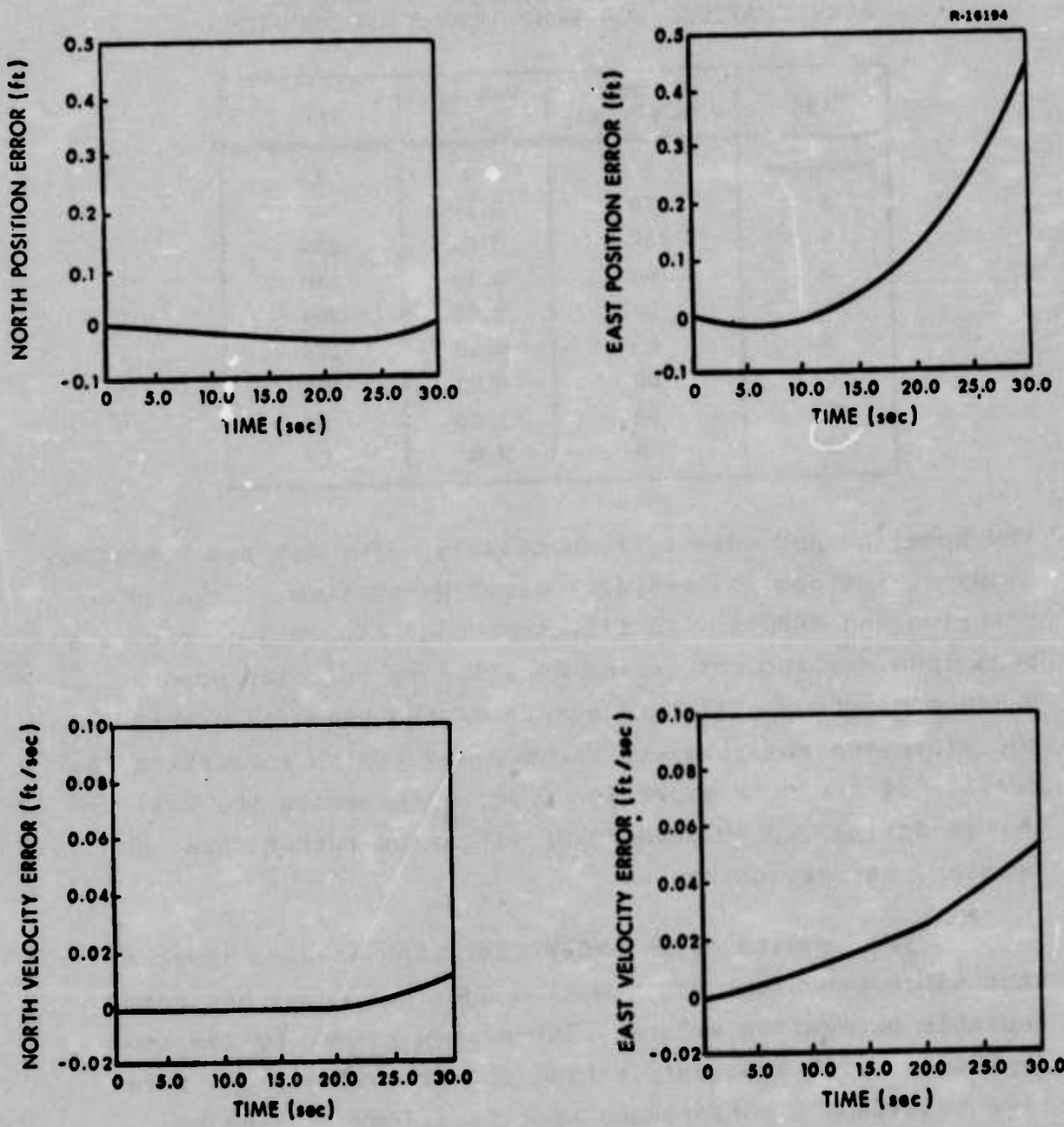

Figure 2.3-2 Baseline Single-Trial Navigation Errors for MCSP Vibration Studies

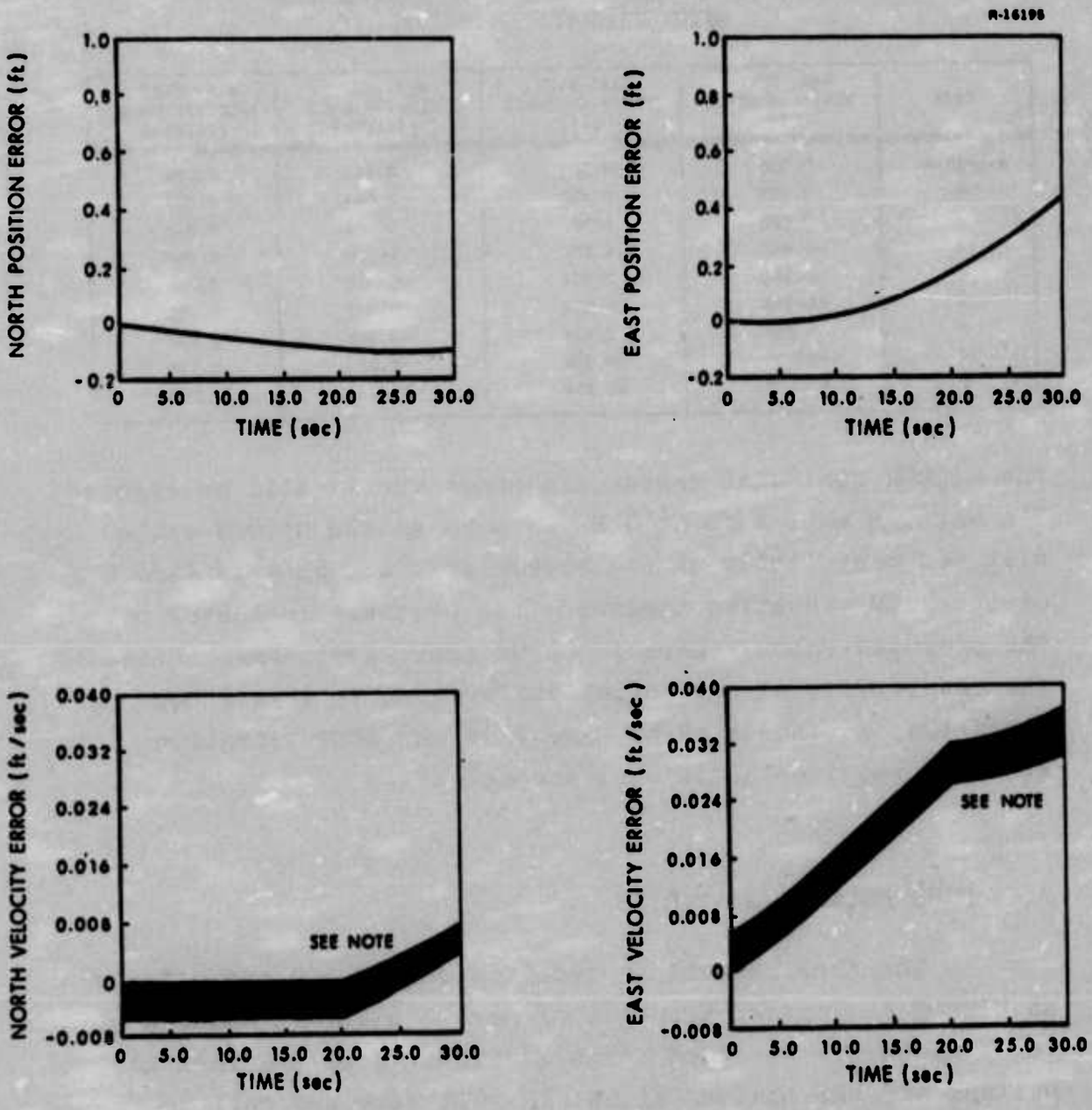

Note: Velocity errors are oscillating at the frequency of the vibro-pendulous motion.

Figure 2.3-3 Case 1 Single-Trial Navigation Errors for MCSP Vibration Studies

TABLE 2.3-2

SINGLE-TRIAL NAVIGATION ERRORS FOR MCSP VIBRATION STUDIES

CASE	MAX. NORTH POSITION ERROR (ft)	MAX. EAST POSITION ERROR (ft)	MAX. NORTH VELOCITY ERROR (ft/sec)	MAX. EAST VELOCITY ERROR (ft/sec)
Baseline	-0.038	0.460	0.012	0.054
1	-0.100	0.423	0.008	0.036
2	-0.060	0.368	0.008	0.032
3	-0.463	0.790	-0.039	0.068
4	-0.161	0.491	-0.012	0.042
5	-0.171	0.545	-0.033	0.078
6	-0.062	0.435	0.014	0.049
7	-78.195	78.008	-5.249	5.875
8	-95.657	95.514	-10.000	11.500

the MICRON equipment inside its shock mounts will be exposed. The maximum amplitude at 5 Hz is 0.2g so the MICRON system will see very little of the motion that was used in Case 8 of the MCSP vibration studies. The resonant frequency of the proposed shock mounts is 20 Hz (Ref. 10); consequently, the sensitivity of navigation performance to this frequency vibration, as indicated by Case 7 of the MCSP vibration studies, requires additional investigation.

2.4 HIGH ROLL RATE STUDIES

The final MCSP investigation considered the effects on MICRON navigation accuracy of severe aircraft maneuvers. These maneuvers included "high-g" linear accelerations and pullups and the maximum allowable roll rate and roll acceleration as delineated by the MICRON specification. To isolate the errors induced by the high roll environment, two trajectories were used in these studies. The two trajectories were identical except that the roll motion environment was included in only one of the trajectories.

The basic trajectory selected was Trajectory 4 described in Ref. 3. Figure 2.4-1 presents an altitude profile of this 30-second trajectory. On a constant northeast heading, the aircraft undergoes a 4g linear acceleration to a velocity of 660 ft/sec followed by a 5g pullup to 45°, and a 6 second climb. The climb is concluded with a 5g turn down maneuver to level unaccelerated flight. During the climb maneuver of Trajectory 4, the total velocity magnitude, V_T, is held constant. The horizontal velocity V_H and the vertical velocity $\dot{h}$ are computed at each iteration of the MCSP Trajectory Generator from the aircraft pitch angle, θ. The equations which determine V_H and $\dot{h}$ are

$$V_H = V_T \cos \theta \qquad (2.4\text{-}1)$$

$$\dot{h} = V_T \sin \theta \qquad (2.4\text{-}2)$$

Table 2.4-1 presents the parameter values which define Trajectory 4 (consult Ref. 3 for a complete description of all the equations used by the MCSP to compute the reference trajectory).

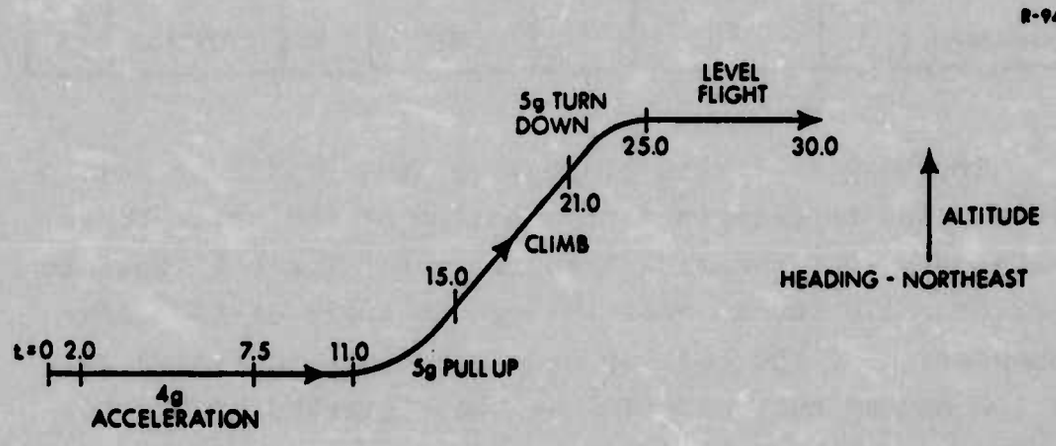

Figure 2.4-1 Trajectory 4 – Acceleration and Pullup

TABLE 2.4-1a

TRAJECTORY 4 INITIAL VALUES

Longitude	λ	-72 degrees	Vertical Velocity	$\dot{h}$	0 ft/sec
Latitude	L	30 degrees	Heading	ψ	$\pi/4$ radians
Altitude	h	0 feet	Pitch Angle	θ	0 radians
Total Velocity	V_T	0 ft/sec	Roll Angle	ϕ	0 radians

TABLE 2.4-1b

TRAJECTORY 4 PARAMETER VALUES VERSUS TIME

TIME (sec)	0-2	2-7.5	7.5-11	11-15	15-21	21-25	25-30
V_T (ft/sec)	0	$V_{T_o} + \int \dot{V}_T \, dt$	660	660	660	660	660
$\dot{V}_T$ (ft/sec^2)	0	120	0	0	0	0	0
ψ (radians)	$\pi/4$	$\pi/4$	$\pi/4$	$\pi/4$	$\pi/4$	$\pi/4$	$\pi/4$
$\dot{\psi}$ (radians/sec)	0	0	0	0	0	0	0
θ (radians)	0	0	0	$\theta_o + \int \dot{\theta} \, dt$	$\pi/4$	$\theta_o + \int \dot{\theta} \, dt$	0
$\dot{\theta}$ (radians/sec)	0	0	0	$\pi/16$	0	$-\pi/16$	0

The high roll rate trajectory (which will be called Trajectory 4a) superimposes roll motion of the aircraft on the maneuvers that comprise Trajectory 4. The roll motions consist of a 1.2 second roll through an angle of 140^o near the completion of the pull-up maneuver shown in Fig. 2.4-1 and a 1.2 second roll of -140^o at the beginning of the leveling maneuver which concludes the climb phase of the trajectory. Table 2.4-2 presents the time histories of the parameters which define Trajectory 4a. The initial conditions for Trajectory 4a are identical to those in Table 2.4-1a for Trajectory 4.

TABLE 2.4-2

TRAJECTORY 4a – ROLL RATE ENVIRONMENT
PARAMETER VALUES VERSUS TIME

TIME (sec)	0.0-2.0	2.0-7.5	7.5-11.0	11.0-14.0	14.0-14.5	14.5-14.7	14.7-15.0
V_T (ft/sec)	0	$V_{T_0} + \int \dot{V}_T \, dt$	660	660	660	660	660
$\dot{V}_T$ (ft/sec^2)	0	120	0	0	0	0	0
ψ (radians)	$\pi/4$	$\pi/4$	$\pi/4$	$\pi/4$	$\pi/4$	$\pi/4$	$\pi/4$
$\dot{\psi}$ (rad/sec)	0	0	0	0	0	0	0
θ (radians)	0	0	0	$\theta_0 + \int \dot{\theta} \, dt$	$\theta_0 + \int \dot{\theta} \, dt$	$\theta_0 + \int \dot{\theta} \, dt$	$\theta_0 + \int \dot{\theta} \, dt$
$\dot{\theta}$ (rad/sec)	0	0	0	$\pi/16$	$\pi/16$	$\pi/16$	$\pi/16$
ϕ (degrees)	0	0	0	0	$\phi_0 + \int \dot{\phi} \, dt$	$\phi_0 + \int \dot{\phi} \, dt$	$\phi_0 + \int \dot{\phi} \, dt$
$\dot{\phi}$ (deg/sec)	0	0	0	0	$\dot{\phi}_0 + \int \ddot{\phi} \, dt$	200	$\dot{\phi}_0 + \int \ddot{\phi} \, dt$
$\ddot{\phi}$ (deg/sec^2)	0	0	0	0	400	0	-400

TABLE 2.4-2 (Continued)

TRAJECTORY 4a – ROLL RATE ENVIRONMENT
PARAMETER VALUES VERSUS TIME

TIME (sec)	15.0-15.2	15.2-20.8	20.8-21.0	21.0-21.3	21.3-21.5	21.5-22.0	22.0-25.0	25.0-30.0
V_T (ft/sec)	660	660	660	660	660	660	660	660
$\dot{V}_T$ (ft/sec^2)	0	0	0	0	0	0	0	0
ϕ (radians)	$\pi/4$	$\pi/4$	$\pi/4$	$\pi/4$	$\pi/4$	$\pi/4$	$\pi/4$	$\pi/4$
$\dot{\psi}$ (rad/sec)	0	0	0	0	0	0	0	0
θ (radians)	$\pi/4$	$\pi/4$	$\pi/4$	$\theta_0 + \int \dot{\theta}\, dt$	$\theta_0 + \int \dot{\theta}\, dt$	$\theta_0 + \int \dot{\theta}\, dt$	$\theta_0 + \int \dot{\theta}\, dt$	0
$\dot{\theta}$ (rad/sec)	0	0	0	$-\pi/16$	$-\pi/16$	$-\pi/16$	$-\pi/16$	0
ϕ (degrees)	$\phi_0 + \int \dot{\phi}\, dt$	140	$\phi_0 + \int \dot{\phi}\, dt$	$\phi_0 + \int \dot{\phi}\, dt$	$\phi_0 + \int \dot{\phi}\, dt$	$\phi_0 + \int \dot{\phi}\, dt$	0	0
$\dot{\phi}$ (deg/sec)	$\dot{\phi}_0 + \int \bar{\phi}\, dt$	0	$\dot{\phi}_0 + \int \bar{\phi}\, dt$	$\dot{\phi}_0 + \int \bar{\phi}\, dt$	-200	$\dot{\phi}_0 + \int \bar{\phi}\, dt$	0	0
$\bar{\phi}$ (deg/sec^2)	-400	0	-400	-400	0	400	0	0

Three MCSP runs were made using Trajectories 4 and 4a to complete the high roll environment studies. Both trajectories were used for cases employing perfect MESG's (no residual drift rate or ARO error) to determine the effects of mechanization errors induced by the severe environments. For the high roll rate trajectory, a single MCSP run was also made using nominal drift rate and ARO error ($|\varepsilon|$ = 0.01 deg/hr, $|\delta\gamma|$ = 0.1 mrad) residuals to describe the MESG. Figures 2.4-2 and 2.4-3 present time histories of the navigation errors during Trajectory 4a for zero and nominal residual errors of the MESG, respectively. Table 2.4-3 presents the terminal navigation errors for all three cases.

The simulation results indicate that the navigation errors due to system mechanization (i.e., the zero MESG error runs) are acceptably small for both the high acceleration and the high roll rate trajectories. Thus, the frequencies chosen for sampling the inertial instruments and solving the navigation equations appear to be adequate for the specified angular rate environment. The differences between the Trajectories 4 and 4a results for the zero MESG error runs indicate that the solution-rate-induced errors are dependent on the motion to which the navigation system is exposed.

Introduction of nominal residual MESG errors into the MCSP yields significantly larger position and velocity errors for the high angular rate trajectory than were observed when there were no MESG errors. Because of the short duration of this trajectory and the assumed zero-valued initial attitude errors, it is likely that the navigation errors are due principally to ARO error. (There has not been sufficient time for residual drift rate to

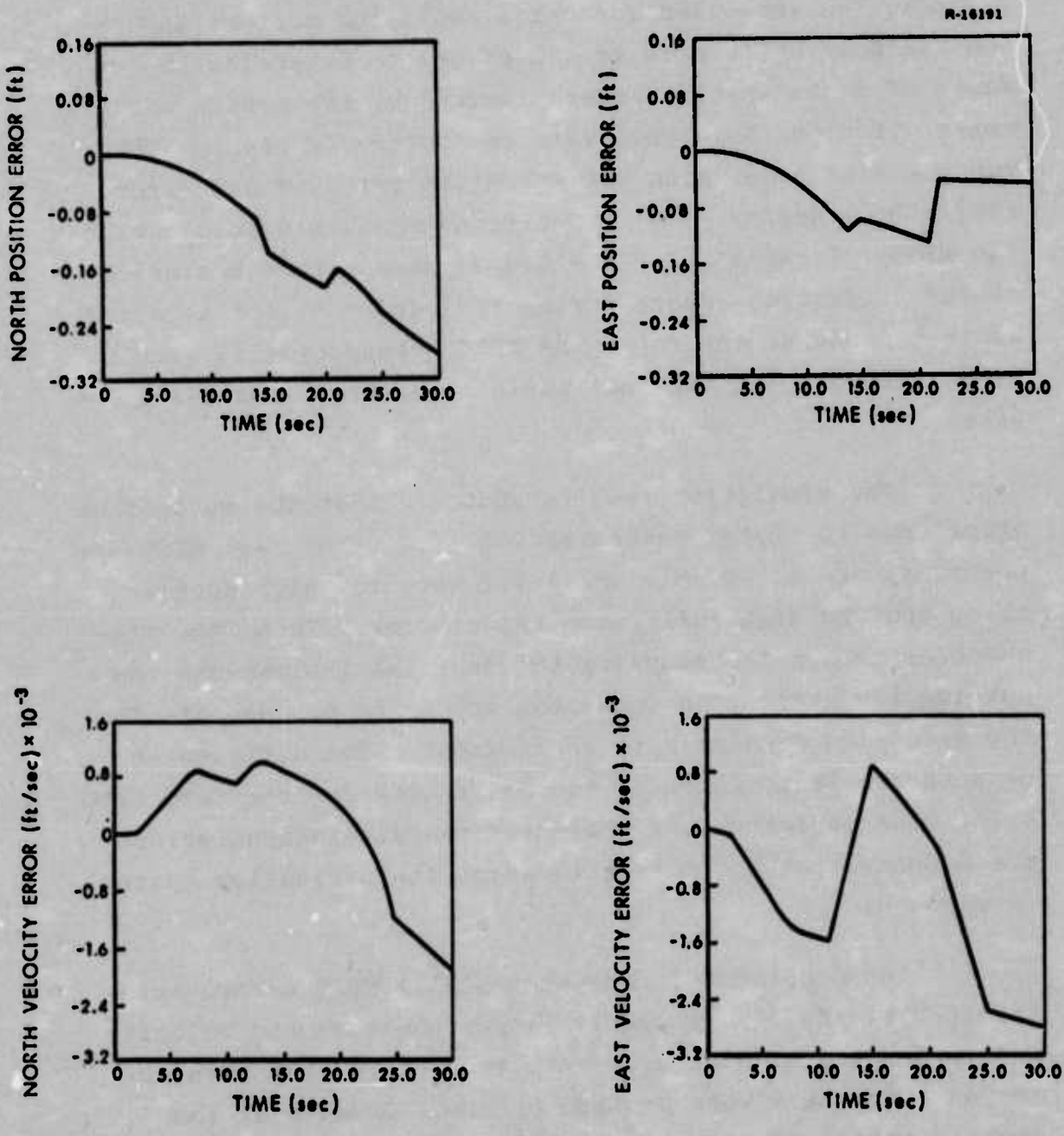

Figure 2.4-2 Navigation Errors for High Roll Rate Trajectory (No MESG Errors)

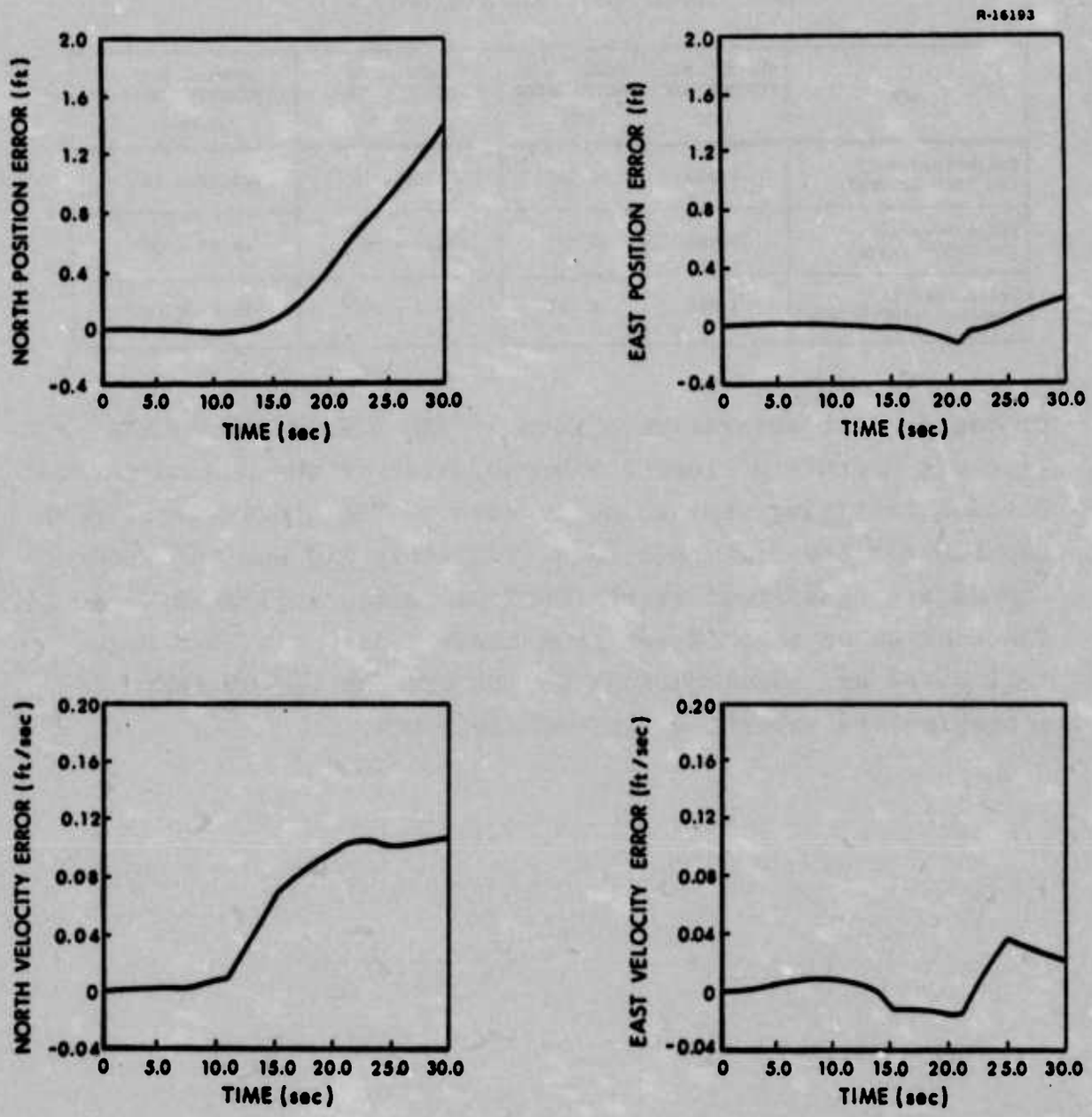

Figure 2.4-3 Single-Trial Navigation Errors for High Roll Rate Trajectory (Nominal MESG)

TABLE 2.4-3

TERMINAL NAVIGATION ERRORS FOR
MCSP HIGH ROLL RATE STUDIES

CASE	TERMINAL NORTH POSITION ERROR (ft)	TERMINAL EAST POSITION ERROR (ft)	TERMINAL NORTH VELOCITY ERROR (ft/sec)	TERMINAL EAST VELOCITY ERROR (ft/sec)
Trajectory 4 (No MESG Errors)	-0.226	-0.285	-0.164×10^{-3}	-2.47×10^{-3}
Trajectory 4a (No MESG Errors)	-0.282	-0.051	-1.92×10^{-3}	-2.80×10^{-3}
Trajectory 4a (Nominal MESG Errors)	1.367	0.195	108.0×10^{-3}	23.0×10^{-3}

propagate into navigation errors.) ARO errors during the aircraft maneuvers cause a misresolution of the sensed acceleration resulting in a velocity error. The single-trial MCSP results for the high roll rate trajectory and nominal MESG errors are consistent with MICRON performance targets (Ref. 5). The conclusion to be drawn from these studies is that high roll rates and accelerations do not prevent MICRON from achieving its specified performance goals.

3. COVARIANCE ERROR ANALYSIS STUDIES

The MICRON Computer Simulation Program (MCSP) which was exercised to generate the results presented in Chapter 2 is a direct simulation of the system navigation equations. It provides the navigation accuracy corresponding to the deterministic set of conditions defined by the program input parameters. To conduct statistical performance analysis studies using the MCSP, it would be necessary to make a large number of computer runs using input error sources provided by random number generators with appropriate statistics. Computing the ensemble statistics of the results of these runs would yield the desired statistical performance prediction. (This technique is called Monte Carlo analysis.)

"Covariance Analysis" is a well-known alternative to Monte Carlo techniques (Ref. 11). Using covariance analysis, a single computer run is used to generate a prediction of the MICRON system performance over an ensemble of similar missions. Covariance analysis evaluation of inertial navigation system performance is a commonly accepted technique which has been used successfully during all stages of navigation system development programs (Refs. 12 and 13). By reviewing the mechanization equations and developing models for MESG residual errors, this chapter will describe the preliminary covariance error analysis program generated by TASC for use in MICRON analysis studies. Since at this stage in MESG instrument development, there has not been sufficient data gathered

to determine valid statistical models for the residual drift rate and ARO errors, it was assumed for the preliminary covariance analysis that the errors were due to miscalibration of some of the simpler drift rate and ARO model terms. The mission assumed for these early analyses was navigation in a stationary laboratory environment. Comparison of the covariance results with lab test data will provide insights allowing improvement of the MESG residual error models during future studies.

During Phase 2 of MICRON development, after the MESG design has been fixed, it is suggested that a Sensor Data Bank be established to collect data on a large number of MESG's. This data should then be used to develop statistical models that accurately describe the residual drift rate and ARO errors of the MESG. These improved models can be used to refine the error analysis program, which was developed as part of the current effort. Expanding the mission scenario capability will allow the evaluation of MICRON performance in any proposed application of interest.

The model of MICRON system performance to be generated during these covariance analysis studies is the kind of system description required for using modern data processing techniques (i.e., Kalman filtering) to integrate MICRON with those navaids that are available in a modern avionics suite. Thus, in addition to providing system performance predictions, development of covariance error analysis tools for MICRON will facilitate future development of aided inertial system mechanizations.

Section 3.1 describes the mechanization proposed for use with the MICRON system. The error equations corresponding to this mechanization are derived in Section 3.2, while the error analysis computer program and some typical covariance results are presented in Section 3.3.

3.1 OVERVIEW OF MECHANIZATION

Prior to describing the error equations for MICRON, it is useful to discuss briefly the navigation mechanization equations which have been implemented. Although MICRON is a strapdown system, the MESG rotors remain fixed in inertial space allowing determination of vehicle attitude directly from the gyros. Consequently, the typical strapdown mechanization problems associated with integrating body rates do not exist in MICRON. The fact that the MICRON accelerometers are mounted directly to the airframe presents a classical strapdown problem of properly integrating the accelerometer outputs to avoid the corrupting effects of vehicle attitude rates.

The MICRON mechanization (Ref. 14) uses three coordinate frames: the MICRON or body frame (designated the M-frame) which is fixed to the vehicle, the S-frame (spin) defined by the rotor spin axes of the two MESG's, and a local-level, free azimuth navigation (N) frame. The M-frame has the input axis of one of the accelerometers along each of its three axes. Also, the case-fixed coordinate frames of both the MESG's are aligned with the M-frame. (When the MESGA multisensor replaces the accelerometers in the final MICRON system, the M-frame will likely be defined by the case-fixed axes of the MESGA.)

The defining axes of the S-frame are $\underline{\gamma}_1$, $\underline{\gamma}_2$, and $\underline{\gamma}_1 \times \underline{\gamma}_2$ where $\underline{\gamma}_i$ is the direction of the rotor spin axis (RSA) of the i^{th} MESG. This frame, which is inertially fixed except for the drift of the RSA's, is not orthogonal because, although the gyros are spun up approximately 90° apart, the two RSA's are not torqued and consequently not constrained to be orthogonal. The fact that the S-frame is not orthogonal

does not present any severe difficulties as long as the appropriate transformations account for the nonorthogonality.

Figure 3.1-1 presents a flowchart describing the MICRON mechanization equations. There are two solution loops associated with this implementation: an inner loop or "fast cycle" which performs time-critical computations 64 times a second and an outer loop or "slow cycle" which executes the remainder of the navigation calculations at 16 times per second (Ref. 14). The strapdown accelerometer problem in MICRON is solved by the fast cycle operations. During each fast cycle, the accelerometer outputs are projected onto the defining axes of the S-frame (determined from the MESG attitude readout), transforming the sensed acceleration during the fast cycle interval into the S-frame. This process creates a "mathematical" accelerometer triad (one accelerometer along each axis of the S-frame) that is essentially inertially fixed and decoupled from vehicle attitude rates (as would be the case on a space stable gimballed platform). The integrated accelerations in the S-frame are then used in the slow loop for the remainder of the navigation computations.

The integrated acceleration in the S-frame is in error due to the effects of accelerometer errors and MESG attitude readout (ARO) errors. Compensation for these effects using the accelerometer and ARO error model coefficients is performed during the slow cycle. Following the compensation of the integrated acceleration in the S-frame, the velocity change is transformed to the local-level N-frame where position and velocity updates occur as shown in Fig. 3.1-1.

The transformation from the S-frame to the N-frame, C_N^S, is computed as a function of the RSA directions coordinatized in the N-frame. (Since the axes of the S-frame are

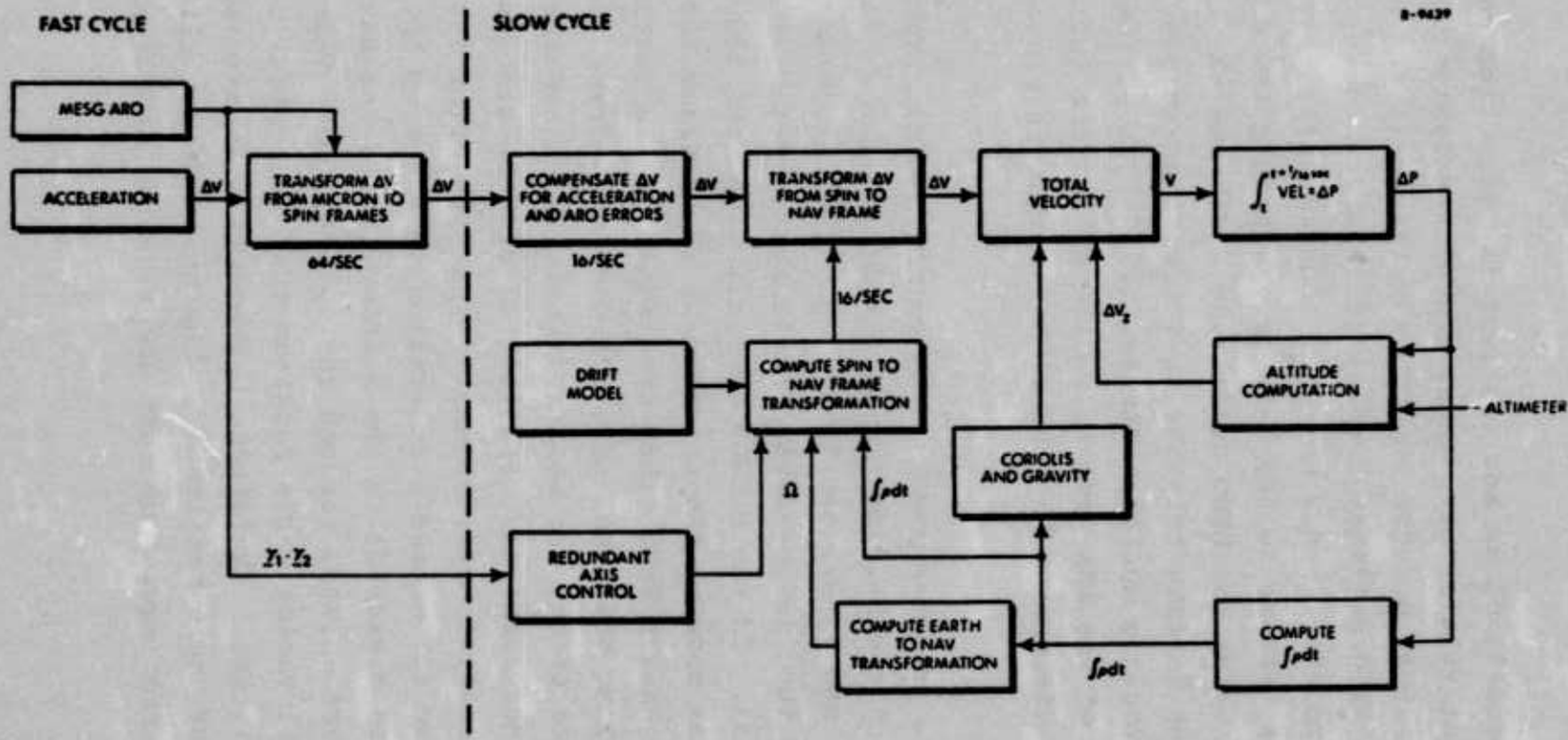

Figure 3.1-1 MICRON Navigation Mechanization Flowchart

not orthogonal, C_N^S is not the familiar direction cosine matrix that relates orthogonal coordinate systems.) It is not possible to measure the RSA directions in the N-frame since the MESG attitude readout is relative to the gyro case which is mounted in the M-frame. Consequently, estimates of the RSA vectors in the N-frame are propagated during the slow loop using the MESG drift rate model and the angular rate of the N-frame relative to inertial space due to earth rate and vehicle motion. The initial values of the N-frame estimates of the RSA vectors (which define the initial value of C_N^S) are determined by the MICRON alignment procedure (see Ref. 14).

The one measurement that can be used to update the estimates of the N-frame RSA direction vectors is the angle between $\underline{\gamma}_1$ and $\underline{\gamma}_2$ defined by $\underline{\gamma}_1 \cdot \underline{\gamma}_2$ (the dot product is a scalar and thus independent of coordinate system in which it is computed). In the MICRON mechanization, the redundant axis control updates the estimate of the N-frame RSA vector for the secondary MESG (that gyro whose RSA is initially horizontal) so that the angle between the N-frame RSA vector estimate tracks the measured angle in a feedback configuration. Redundant axis control, as will be discussed in the error analysis development, forces the error introduced by resolving the sensed acceleration vector from the M-frame (where it is measured) to the N-frame (where the navigation equations are solved) through the nonorthogonal S-frame to be the small vector angle rotation that is typical of all inertial systems. (Reference 9 presents a discussion of small vector angle rotations.) The next section will develop the error equations that describe the MICRON system.

3.2 ERROR EQUATION DEVELOPMENT

The dynamic propagation of basic error sources into INS system errors is well known (Refs. 9 and 15). It has been shown that, for any dynamically exact implementation of the terrestrial navigation equations, the propagation of inertial instrument errors and gravity model errors can be viewed independently of the particular mechanization that actually appears in the system (Ref. 16). Consequently, the error equations can be written in any convenient coordinate system as long as care is taken to properly identify the specific driving error sources for the system and mechanization being studied.

In addition to instrument induced dynamic errors which are independent of the particular mechanization, there also exist implementation errors (caused by computer roundoff, numerical inaccuracy, and solution rates) which will depend on the particular mechanization employed. The covariance error analysis technique is not well suited for investigating the effects of implementation errors; and thus, they will not be considered. The MCSP, which duplicates the MICRON mechanization, has been used to investigate these errors (Ref. 3).

The philosophical approach to error equation development taken in Refs. 9 and 15 requires the identification of three coordinate frames, ideally coincident but actually differing by small angles due to navigation errors. These frames are: the inertial (often called the platform) frame which is an inertially stabilized frame where the accelerometer outputs are measured, the computation frame in which the navigation equations are solved, and the true frame in which it is desired to mechanize the navigation equations. Summarizing the results of the derivation, the dynamic equations of INS error propagation can be written as

$$\frac{d}{dt}\left(\delta \underline{r}^L\right) = -\underline{\omega}_{EL}^L \times \delta \underline{r}^L + \delta \underline{v}^L \qquad (3.2\text{-}1)$$

$$\frac{d}{dt}\left(\delta \underline{v}^L\right) = -\left(2\underline{\omega}_{IE}^L + \underline{\omega}_{EL}^L\right) \times \delta \underline{v}^L - \underline{\psi}^L \times \underline{f}^L + \delta \underline{g}^L + \delta \underline{f}^L \qquad (3.2\text{-}2)$$

$$\frac{d}{dt}\left(\underline{\psi}^L\right) = -\left(\underline{\omega}_{IE}^L + \underline{\omega}_{EL}^L\right) \times \underline{\psi}^L + \underline{\varepsilon}^L \qquad (3.2\text{-}3)$$

where

$\delta \underline{r}$ = INS position error

$\delta \underline{v}$ = INS velocity error

$\underline{\psi}$ = the small vector angle rotation such that if the computation frame were rotated about the $\underline{\psi}$ direction by an angle ψ it would be brought into coincidence with the inertial (or platform) frame.

$\underline{\omega}_{EL}$ = angular rate of the L-frame with respect to (w.r.t.) an earth-fixed axis set

$\underline{\omega}_{IE}$ = angular rate of an earth-fixed axis set w.r.t. inertial space

$\delta \underline{g}$ = error in calculation of gravity

$\delta \underline{f}$ = error in acceleration sensing

$\underline{\varepsilon}$ = gyro drift rate

The superscript "L" refers to the coordinate frame in which the error analysis is to be performed. The driving error terms $\delta \underline{g}$, $\delta \underline{f}$ and $\underline{\varepsilon}$ depend on the particular system and mechanization being studied and will be defined for the MICRON system in the remainder of this section.

The MICRON error equations will be written in a north-slaved local-level coordinate frame. Although MICRON is mechanized using a local-level wander azimuth system (since it does not exhibit the polar singularity observed in north-slaved systems), it is desirable to write the error equations

in a north-slaved frame since several error sources (gravity errors and initial condition errors) are most easily modeled in a north-slaved frame. Also, output errors (navigation position and velocity) are usually cited in this frame. Thus, for the MICRON error equation development, the L-frame used in Eqs. (3.2-1) to (3.2-3) will be the local-level north slaved (NED) coordinate system with its x-axis north, y-axis east, and z-axis down. Section 3.2.1 will present the form of the velocity error driving terms [$\delta\underline{g}$ and $\delta\underline{f}$ in Eq. (3.2-2)] for the MICRON system while Section 3.2.2 will derive the MICRON gyro drift rate expression which drives the $\dot{\underline{\psi}}$ equation [Eq. (3.2-3)].

3.2.1 MICRON Gravity Calculation and Acceleration Sensing Errors

Accelerometers measure specific force, $\underline{f}$, defined as

$$\underline{f} = \underline{a} - \underline{g} \qquad (3.2\text{-}4)$$

where $\underline{a}$ is the inertial acceleration and $\underline{g}$ is the gravity vector. Since the inertial navigation computations of position and velocity (which consist of integrating Newton's second law of motion) require knowledge of the inertial acceleration, $\underline{a}$, it is necessary that the system mechanization estimate $\underline{g}$ using a gravity model and the indicated vehicle position. While avoiding a detailed discussion of the gravity model that is implemented in MICRON, it is possible to identify two classes of gravity errors, $\delta\underline{g}$, which drive the error equations. These classes of errors are: (1) errors due to evaluating the gravity model at the erroneous navigator-indicated position, and (2) errors caused by a difference between the true gravity and the gravity model evaluated when position is known exactly.

It can be shown that in the L-frame, the gravity error due to the INS position error can be expressed as

$$\delta \underline{g}^L = \frac{g_o}{R} \begin{bmatrix} -1 & 0 & 0 \\ 0 & -1 & 0 \\ 0 & 0 & 2 \end{bmatrix} \delta \underline{r}^L \qquad (3.2\text{-}5)$$

where g_o is the nominal value of gravity and R is the radius of the earth. Inserting Eq. (3.2-5) into Eq. (3.2-2) and combining with Eq. (3.2-1) demonstrates the classical oscillation of horizontal position error at the Schuler frequency $\omega_s = \sqrt{g_o/R}$ and the instability of vertical channel navigator errors. The vertical channel is stabilized using an altimeter and feeding the difference between the INS vertical position and the altimeter output back through appropriate gains to the inputs of the vertical position and velocity integrators. The altimeter output is not used in the gravity calculation for MICRON. This stabilization technique introduces altimeter errors into the error equations for the vertical channel. Appendix A presents a derivation of the vertical channel error equations resulting from altimeter damping.

Gravity errors due to differences between the true gravity and the modeled gravity when the position is known exactly are called gravity anomalies and deflections of the vertical. Gravity anomalies are errors in the magnitude of the model estimate while deflections of the vertical are errors in the direction of the gravity vector. TASC has conducted extensive studies directed both at developing statistical descriptions of gravity model errors (Ref. 17) and investigating the effects of these errors on INS performance accuracy (Ref. 18). For a moderate accuracy inertial system such as MICRON, gravity anomalies and deflections

of the vertical are not expected to be dominant error sources. Consequently, these $\delta\underline{g}$ error terms were not included in the preliminary MICRON error equations.

The derivation of the acceleration sensing errors, $\delta\underline{f}^L$, which drive the velocity error equation [Eq. (3.2-2)] requires careful review of the MICRON mechanization to insure that the errors are properly transformed from the coordinate frame in which they occur into the L-frame where the error equations are being written. It will be shown that the MESG Attitude Readout errors drive the error equations in a similar manner to accelerometer misalignments.

To avoid confusion caused by the large number of different coordinate frames, it is useful to associate the coordinate frames in the MICRON mechanization as described in Section 3.1 with the three coordinate frames that formed the basis of the error equation development. The MICRON S-frame defined by the spin axis vectors of the two MESG's corresponds to the inertial (platform) frame while the local-level, azimuth wander N-frame can be viewed as the computation frame. The true frame is that frame in which it is desired to mechanize the MICRON navigation equations and thus is defined by the actual vehicle position. Although it does not correspond to one of the frames used to derive the error equations, the body fixed M-frame (see Section 3.1) is the coordinate system in which all the inertial sensors are mounted and thus is the frame where the instrument errors actually occur.

As discussed in Section 3.1, the MICRON mechanization solves the strapdown accelerometer problem by projecting the accelerometer outputs, $\underline{f}^M$, onto $\underline{\gamma}_1$, $\underline{\gamma}_2$ and $\underline{\gamma}_1 \times \underline{\gamma}_2$ creating a mathematical accelerometer triad in the inertially stable

S-frame. The specific force in this S-frame, $\underline{f}^S$, can be related to the accelerometer outputs (i.e., specific force in the M-frame), $\underline{f}^M$, by

$$\underline{f}^S = \begin{bmatrix} \underline{f}^M \cdot \underline{\gamma}_1^M \\ \underline{f}^M \cdot \underline{\gamma}_2^M \\ \underline{f}^M \cdot \left(\underline{\gamma}_1^M \times \underline{\gamma}_2^M\right) \end{bmatrix} = C_M^S \, \underline{f}^M \qquad (3.2\text{-}6)$$

where

$$C_M^S = \left[\underline{\gamma}_1^M \;\vdots\; \underline{\gamma}_2^M \;\vdots\; \left(\underline{\gamma}_1^M \times \underline{\gamma}_2^M\right)\right]^T \qquad (3.2\text{-}7)$$

The acceleration sensing errors relative to the platform frame (which, for MICRON, is the S-frame) determine the system driving errors $\delta\underline{f}$ in Eq. (3.2-2).

Perturbing Eq. (3.2-6) yields

$$\delta\underline{f}^S = C_M^S \left(\delta\underline{f}^M + \delta C_m^S \, \underline{f}^M\right) \qquad (3.2\text{-}8)$$

$\delta\underline{f}^M$ is the accelerometer instrument error and δC_M^S is the error introduced by the MESG ARO errors in constructing the mathematical accelerometer triad along the axes of the S-frame. The errors associated with the accelerometer are scale factor and misalignments, random bias, and a first order Markov noise error. Including these terms, it is possible to express the accelerometer instrument errors, $\delta\underline{f}^M$, as

$$\delta\underline{f}^M = K \, \underline{f}^M + \underline{\nabla}_b + \underline{\nabla}_r \qquad (3.2\text{-}9)$$

The matrix K models scale factor and misalignment errors while $\underline{\nabla}_b$ and $\underline{\nabla}_r$ represent the bias and Markov noise components of the accelerometer errors.

The MESG ARO errors that remain following compensation cause the readout position of the rotor spin axis (RSA) to be misaligned from its true position. Thus, projecting the accelerometer data onto these misaligned RSA vectors will result in an effective misalignment of the mathematical accelerometer triad. It is this error source which is modeled by the $\delta C_M^S \, \underline{f}^M$ term in Eq. (3.2-8). By perturbing Eq. (3.2-7) and retaining only first order terms, it is possible to compute δC_M^S as

$$\delta C_M^S = \left[\delta \underline{\gamma}_1^M \vdots \delta \underline{\gamma}_2^M \vdots \left(\underline{\gamma}_1^M \times \delta \underline{\gamma}_2^M \right) + \left(\delta \underline{\gamma}_1^M \times \underline{\gamma}_2 \right) \right]^T \tag{3.2-10}$$

where $\delta \underline{\gamma}_1^M$ and $\delta \underline{\gamma}_2^M$ represent the residual ARO error of the primary and secondary MESG's, respectively. Using Eq. (3.2-10)

$$\delta C_M^S \, \underline{f}^M = \begin{bmatrix} \underline{f}^{M^T} \\ 0 \\ \left(\underline{\gamma}_2^M \times \underline{f}^M \right)^T \end{bmatrix} \delta \underline{\gamma}_1^M + \begin{bmatrix} 0 \\ \underline{f}^{M^T} \\ \left(\underline{f}^M \times \underline{\gamma}_1^M \right)^T \end{bmatrix} \delta \underline{\gamma}_2^M \tag{3.2-11}$$

The form of the statistical models describing the residual ARO errors, $\delta \underline{\gamma}$, needed to allow the use of Eq. (3.2-11) in the MICRON error analysis are not yet well defined (due to insufficient MESG data). For the preliminary development of the error analysis computer program that was performed as part of the current effort, the residual ARO errors were assumed to be due to miscalibration of some of the principal terms in the ARO compensation model (Ref. 3). During future MICRON analysis studies, when the MESG design has been frozen and there is data available on a large

number of gyros, it is suggested that investigations be performed to develop valid models to describe the residual MESG instrument errors.

The acceleration sensing errors described by Eq. (3.2-8) are coordinatized in the S-frame. Since it has been decided to perform the MICRON error analysis in the L-frame, it is necessary to transform $\delta\underline{f}^S$ into the L-frame before it is used in Eq. (3.2-2). Thus

$$\begin{aligned}\delta\underline{f}^L &= C_S^L\, C_M^S \left(\delta\underline{f}^M + \delta C_M^S\, \underline{f}^M\right) \\ &= C_M^L \left(\delta\underline{f}^M + \delta C_M^S\, \underline{f}^M\right)\end{aligned} \tag{3.2-12}$$

The transformation C_M^L, which relates the body-fixed M-frame to the local-level, north slaved L-frame, will be a function of the vehicle attitude and consequently will depend on the trajectory for which the error analysis is performed.

Summarizing by substituting Eqs. (3.2-9) and (3.2-11) into Eq. (3.2-12), it is possible to express the acceleration sensing errors (accelerometer and ARO errors) that drive the velocity error equation [Eq. (3.2-2)] for the MICRON system as

$$\delta\underline{f}^L = C_M^L \left\{ K\,\underline{f}^M + \underline{v}_b + \underline{v}_r + \begin{bmatrix} \underline{f}^{M^T} \\ 0 \\ \left(\underline{\gamma}_2^M \times \underline{f}^M\right)^T \end{bmatrix} \delta\underline{\gamma}_1^M + \begin{bmatrix} 0 \\ \underline{f}^{M^T} \\ \left(\underline{f}^M \times \underline{\gamma}_1\right)^T \end{bmatrix} \delta\underline{\gamma}_2^M \right\} \tag{3.2-13}$$

where the models for the residual ARO error $\delta\underline{\gamma}_1^M$ and $\delta\underline{\gamma}_2^M$ remain to be defined. The models that were used during the development of the error analysis computer program will be

presented in Section 3.3.1. Appendix B will delineate the system state vector and its dynamics matrix that described the MICRON navigation errors.

3.2.2 Gyro Drift Error Propagation

In the previous section, the error sources which drive the velocity error equation for the MICRON system were identified. To complete the MICRON error analysis equations, it is necessary to derive the driving error sources for the $\underline{\psi}$ angle equation [Eq. (3.2-3)]. Ref. 9, which presents a detailed derivation of the $\underline{\psi}$ angle equation, views the vector angle rotation, $\underline{\psi}$, as descriptive of the error introduced in transforming a vector (in particular, the sensed acceleration vector) from the stabilized platform frame to the computation frame. This error is caused by an error in the computer's estimate of the transformation from the platform frame to the computation frame.

For the MICRON mechanization, the S-frame defined by the MESG RSA direction vectors has been identified as the platform frame while the computation frame is the local-level wander azimuth N-frame defined by the computed vehicle position and wander angle. Thus, $\underline{\psi}$ describes the error in the estimate of S-frame basis vectors (i.e., the RSA vectors) in N-frame coordinates since it is the estimates of the spin vectors (in the N-frame) which define $\hat{C}_S^N$. The estimation process assumes that the RSA's are fixed relative to inertial space, except for the redundant axis control and the modeled gyro drift. Consequently, residual (unmodeled) drift of the MESG spin axes relative to inertial space is the only system error source dynamically driving $\underline{\psi}$.

The redundant axis control constrains the estimate of the spin axis vector for the secondary MESG (the primary

gyro's RSA is initially vertical while the RSA of the secondary MESG is horizontal and forward along the aircraft longitudinal axis) in N-frame coordinates, $\underline{S}_{N2}$. As is demonstrated in Appendix C, the redundant axis control adjusts $\underline{S}_{N2}$ in the $\underline{S}_{N1}$ - $\underline{S}_{N2}$ plane so that the scalar product $\underline{S}_{N1} \cdot \underline{S}_{N2}$ equals $\underline{\gamma}_{C1} \cdot \underline{\gamma}_{C2}$ which is determined from the compensated readout of the RSA vectors. Consequently, for the secondary gyro only that residual drift which moves $\underline{S}_{N2}$ out of the $\underline{S}_{N1}$ - $\underline{S}_{N2}$ plane will affect the $\underline{\psi}$ angle.

$\delta\underline{P}_1$ and $\delta\underline{P}_2$ are now defined as the residual drift rate vectors, coordinatized in the MESG case coordinates (M-frame), of the primary and secondary gyros, respectively. It is then possible, using the constraint imposed by redundant axis control, to determine an expression for $\underline{\varepsilon}$ [Eq. (3.2-3)] in terms of $\delta\underline{P}_1$ and $\delta\underline{P}_2$. This expression is

$$\underline{\varepsilon}^M = \left(I - \underline{\gamma}_1^M \underline{\gamma}_1^{M^T}\right) \delta\underline{P}_1 + \underline{\gamma}_1^M \underline{\gamma}_1^{M^T} \delta\underline{P}_2 \qquad (3.2\text{-}14)$$

since residual drift rate of the primary gyro in the $\underline{\gamma}_1^M$-direction does not lead to any error; and, due to redundant axis control, only the residual drift rate about the $\underline{\gamma}_1^M$-direction of the secondary MESG causes $\underline{\psi}$ angle errors.

Since the error analysis is to be performed in the L-frame, it is necessary to transform the drift rate vector in Eq. (3.2-14) into the L-frame. Thus

$$\underline{\varepsilon}^L = C_M^L \left[\left(I - \underline{\gamma}_1^M \underline{\gamma}_1^{M^T}\right) \delta\underline{P}_1 + \underline{\gamma}_1^M \underline{\gamma}_1^{M^T} \delta\underline{P}_2\right] \qquad (3.2\text{-}15)$$

Summarizing the results of this section, Fig. 3.2-1 presents the MICRON error propagation equations in vector-matrix form. The next section will describe the computer

$$\frac{d}{dt}\left(\delta \underline{r}^L\right) = -\underline{\omega}_{EL}^L \times \delta \underline{r}^L + \delta \underline{v}^L$$

$$\frac{d}{dt}\left(\delta \underline{v}^L\right) = -\left(2\,\underline{\omega}_{IE}^L + \underline{\omega}_{EL}^L\right) \times \delta \underline{v}^L - \underline{\psi}^L \times \underline{f}^L + \frac{g_o}{R}\begin{bmatrix} -1 & 0 & 0 \\ 0 & -1 & 0 \\ 0 & 0 & 2 \end{bmatrix} \delta \underline{r}^L$$

$$+ C_M^L \left\{ K \underline{f}^M + \underline{\nu}_b + \underline{\nu}_r + \begin{bmatrix} \underline{f}^{M^T} \\ 0 \\ \left(\underline{Y}_2^M \times \underline{f}^M\right)^T \end{bmatrix} \delta \underline{Y}_1^M + \begin{bmatrix} 0 \\ \underline{f}^{M^T} \\ \left(\underline{f}^M \times \underline{Y}_1\right)^T \end{bmatrix} \delta \underline{Y}_2^M \right\}$$

$$\frac{d}{dt}\left(\underline{\psi}^L\right) = -\left(\underline{\omega}_{IE}^L + \underline{\omega}_{EL}^L\right) \times \underline{\psi}^L + C_M^L \left[\left(I - \underline{Y}_1^M \underline{Y}_1^{M^T}\right)\delta \underline{P}_1 + \underline{Y}_1^M \underline{Y}_1^{M^T}\, \delta \underline{P}_2\right]$$

where

$\delta \underline{r}$	=	INS position error
$\delta \underline{v}$	=	INS velocity error
$\underline{\psi}$	=	misalignment between computer and inertial frames
$\underline{f}$	=	specific force vector
$\underline{\omega}_{EL}^L$	=	angular rate of L-frame w.r.t. earth-fixed frame in L-frame coordinates
$\underline{\omega}_{IE}^L$	=	angular rate of earth-fixed frame w.r.t. inertial space in L-frame coordinates
K	=	accelerometer scale factor and misalignment matrix
$\underline{\nu}_b$	=	bias accelerometer error vector
$\underline{\nu}_r$	=	random accelerometer error vector
$\underline{Y}_1$	=	RSA vector for MESG No. 1
$\underline{Y}_2$	=	RSA vector for MESG No. 2
C_M^L	=	transformation from M-frame to L-frame
$\delta \underline{Y}_1$	=	residual ARO error for MESG No. 1
$\delta \underline{Y}_2$	=	residual ARO error for MESG No. 2
$\delta \underline{P}_1$	=	residual drift rate vector for MESG No. 1
$\delta \underline{P}_2$	=	residual drift rate vector for MESG No. 2

*These equations do not include vertical channel damping errors (see Appendix A).

Figure 3.2-1 MICRON Navigation Error Propagation Equations*

program which was used for the MICRON error analysis studies and will present some of the preliminary results that were generated.

3.3 ERROR ANALYSIS COMPUTER PROGRAM

To allow prediction of the MICRON system performance, the covariance equations corresponding to the error dynamics derived in Section 3.2 have been coded, forming the error analysis computer program. The preliminary version of this program (which is described in this section) is specialized to a stationary laboratory environment with discrete attitude changes and assumes that the residual drift rate and ARO errors are due to miscalibration of terms appearing in the compensation models. During future MICRON error covariance simulation studies, it is suggested that the computer program be refined to incorporate the trajectories of planned MICRON applications and to include more accurate descriptions of the residual instrument errors as they become available.

The state vector description of MICRON system errors used in the error analysis computer program consists of 45 elements. Nine of these states (3 position errors, 3 velocity errors, and 3 ψ-angles) represent the system accuracy while the remaining 36 states model the error sources which drive the system states. Table 3.3-1 presents a list of the error sources included in the covariance analysis program and the number of states which are required to model these errors.

As was presented in Section 3.2, the residual drift rate and ARO errors of the individual MESG's propagate into system errors as a function of the RSA directions. Also, some of the models used to describe residual instrument

TABLE 3.3-1

MICRON ERROR ANALYSIS PROGRAM STATES

DESCRIPTION	NUMBER OF INDIVIDUAL SOURCES	NUMBER OF ADDED STATES
MICRON Position Error	3	3
MICRON Velocity Error	3	3
ψ-Angle Misalignments	3	3
Accelerometer Bias Errors	3	3
Accelerometer Random Errors	3	3
Accelerometer Scale Factor Errors	3	1
Altimeter Error	1	1
ARO Scale Factor Errors	6 (3 for each MESG)	15
Case-Fixed Bias Drifts	6 (3 for each MESG)	9
Random Drift	3	3
Acceleration Sensitive Drift Miscalibration	1	1
Acceleration Sensitive Drift Miscompensation Due to Accelerometer Error	1	0
TOTAL	42	45

errors depend on the RSA direction. Consequently, the dynamics of many of the system driving states are related to the motion of the inertially-fixed RSA's which, for the stationary laboratory environment, move at earth rate relative to the L-frame where the error analysis is to be performed. The fact that the gravity vector is constant and oriented along one of the axes of the local-level L-frame has been used to reduce the number of states required to describe the MICRON

error sources. When, during future studies, vehicle motion is added to the error analysis program, it is likely that additional states will be required to properly account for the effects of the MICRON error sources.

Section 3.3.1 describes the instrument residual error models that have been used. (Appendix B presents the state vector and dynamics matrix.) Section 3.3.2 presents the computer program description while Section 3.3.3 presents some of the results of the checkout runs that were performed with the program.

3.3.1 Residual Instrument Errors

A brief description of the sensor errors that have been included in the error analysis program is presented. For drift rate and ARO errors, the selected models have been determined by ascribing the residual errors to miscalibration of dominant compensation terms. During future MICRON Analysis efforts, it is suggested that test data from a large number of MESG's be evaluated to determine valid statistical descriptions of residual drift rate and ARO errors.

Accelerometer Errors – Three types of errors have been associated with the accelerometers for the MICRON system model used in the error analysis program. These are bias, scale factor and random errors. The random accelerometer errors are modeled by a first order Markov process. Although the error equations are written in the L-frame, the accelerometers are physically mounted in the M-frame (see Section 3.2). Consequently, the program input parameters which describe the accelerometer errors are defined relative to the M-frame, and the error analysis program must compute the equivalent errors in the L-frame for use in the

MICRON error equations. It is thus possible to express the total accelerometer error vector in the L-frame, $\underline{\nabla}_T^L$, as

$$\underline{\nabla}_T^L = C_M^L \left[\underline{\nabla}_b^M + \underline{\nabla}_r^M + \delta C_{ASF} \, \underline{g}^M \right] \qquad (3.3\text{-}1)$$

where $\underline{\nabla}_b^M$ represents the bias errors, $\underline{\nabla}_r^M$ models the random acclerometer errors, and δC_{ASF} is a diagonal matrix of scale factor errors for the three accelerometers.

Altimeter Errors – The typical errors that occur in altimeters are bias and scale factor. For the stationary laboratory environment, the altitude is constant and the scale factor error in the altimeter is constant. Thus, it is possible to model all the altimeter errors for this case as a single bias error.

Attitude Readout Errors – Since scale factor errors are one of the dominant sources of ARO error in the MESG (Ref. 6), it was decided to characterize the residual readout errors using this form. As a result of this model selection, the ARO error in the M-frame, $\delta\underline{\gamma}_i^M$, that appears in Eq. (3.2-11) was expressed as

$$\delta\underline{\gamma}_i^M = \begin{bmatrix} \delta C_{ix} & 0 & 0 \\ 0 & \delta C_{iy} & 0 \\ 0 & 0 & \delta C_{iz} \end{bmatrix} \underline{\gamma}_i \; ; \quad i=1,2 \qquad (3.3\text{-}2)$$

Because the ARO errors propagate into MICRON velocity errors as functions of the RSA direction in the case [see Eq. (3.2-13)], the states in the error analysis program that model these errors are products of the terms in Eq. (3.2-2) and the components of the $\underline{\gamma}$-vectors. (Appendix B enumerates these states

and their associated dynamics.) The initialization portion of the computer program accepts, as input parameters, the covariance statistics of the δC_{ij}'s in Eq. (3.3-2) and constructs the appropriate states required to implement the effects of ARO errors as described in Section 3.2.

Drift Rate Errors – The model for residual drift rate of the MESG spin axis includes miscalibration of the case-fixed bias and axial mass unbalance drift rate coefficients (see Ref. 3 for a discussion of these drift rate terms) and random drift rate effects. An additional drift rate error that results from computing the axial mass unbalance drift rate compensation using the sensed acceleration is also modeled. (Since the sensed acceleration is corrupted by accelerometer errors, using the sensed acceleration in the drift rate compensation introduces residual drift rate errors which drive the MICRON navigation errors.)

The parameters which describe the statistics of the case-fixed bias drift rates are entered into the error analysis program in the M-frame. The initialization module of the program then computes the appropriate covariance matrix in the L-frame to model these errors. To simplify the models, it was assumed that the axial mass unbalance drift rate coefficient and its calibration error were the same for both MESG's. The random drift rate, which was modeled as a Markov process, was entered into the program in the L-frame. It is possible to summarize the model for residual drift rate as

$$\underline{\varepsilon}^L = \underline{\varepsilon}_r^L + \underline{\varepsilon}_{B1}^L + \left[\underline{\gamma}_1 \, \underline{\gamma}_1^T \left(\underline{\varepsilon}_{B2} - \underline{\varepsilon}_{B1}\right)\right]^L + \delta P_g \, \underline{g}^L + P_g \, \underline{\nabla}^L \tag{3.3-3}$$

where $\underline{\varepsilon}_{B1}$ and $\underline{\varepsilon}_{B2}$ are the residual case-fixed drift rate vectors of the primary and secondary MESG's. P_g is the axial mass unbalance coefficient and δP_g is the calibration error in this coefficient. $\underline{\varepsilon}_r^L$ is the Markov drift rate vector.

3.3.2 Program Description

The structure of the error analysis computer program is quite simple as can be seen from the flowchart which appears in Fig. 3.3-1. The modules which compose the program perform initialization, transition matrix computation, updates to model a change in MICRON attitude, covariance propagation, and data output. The initialization module accepts the input data which describes the MICRON error parameters and constructs an initial covariance matrix, P_0, to represent the initial conditions on the system state vector. Also, the system dynamics matrix, F, and the continuous noise matrix, Q, are assembled; and, data defining the initial navigation attitude, program time step, final time, and discrete attitude changes are input and stored for use by other modules.

The two central modules of the error analysis program are those which compute the transition matrix and the discrete noise matrix and which propagate the covariance matrix. The equations which accomplish these operations are well-known (Ref. 11), but will be repeated here for completeness. The transition matrix, Φ, is computed as:

$$\Phi = e^{F\Delta t} \qquad (3.3\text{-}4)$$

where Δt is the time step size for the covariance propagation. The discrete noise matrix, Q_k, is defined by:

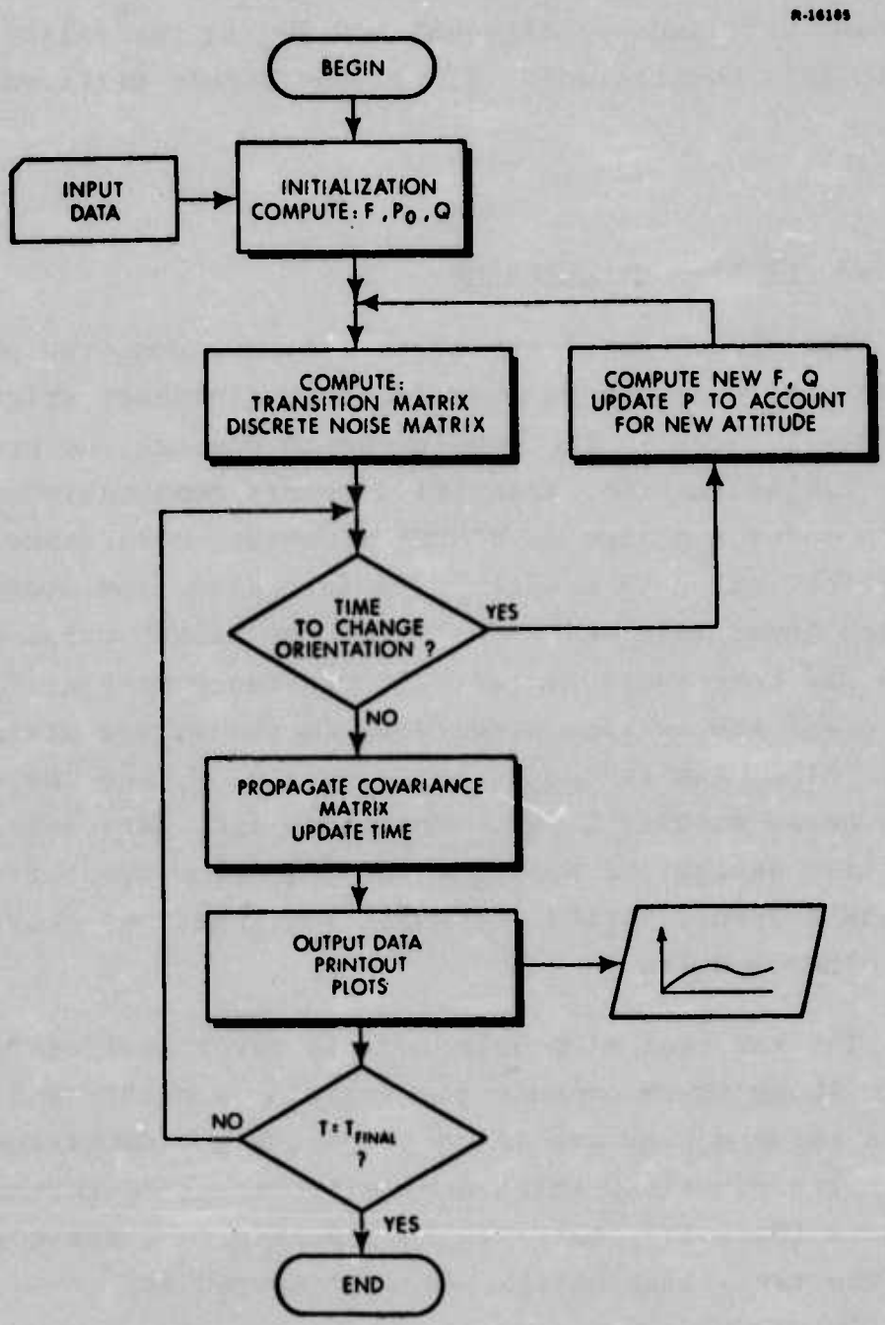

Figure 3.3-1 Flowchart for Error Analysis Computer Program

$$Q_k = \int_0^{\Delta t} \Phi \, Q \, \Phi^T \, dt \qquad (3.3\text{-}5)$$

and the covariance matrix is propagated from t_k to t_{k+1} ($t_{k+1} = t_k + \Delta t$) by:

$$P_{k+1} = \Phi \, P_k \, \Phi^T + Q_k \qquad (3.3\text{-}6)$$

The MICRON error analysis computer program assumes that the MICRON system is operating in a stationary laboratory environment, except for discrete changes in attitude. The time at which an attitude change is to occur and the parameters that describe the attitude change are program inputs. The MICRON error propagation is dependent on the orientation of the RSA's relative to the gyro case, and consequently, a change in MICRON attitude alters the driving error sources. The attitude change module properly updates the system covariance matrix and recomputes the dynamics and noise matrices to model the effects of an attitude change on the MICRON navigation errors.

The final module of the error analysis program is an output module. It prints the diagonal elements of the covariance matrix at each time step and stores those data points that are to be plotted. Typically, plots have been generated for the time history of the rms position, velocity, and ψ-angle errors of the MICRON system in response to the specified instrument error sources. The next section will present the results of several of the checkout runs that were made to exercise the error analysis program.

3.3.3 Covariance Error Analysis Results

The error analysis computer program described in the previous section has been coded and exercised to verify its

proper operation. Program checkout was accomplished by setting all error sources and initial condition errors to zero except one and ascertaining that the single error source induced the appropriate error behavior. Those errors which were investigated during program checkout included initial position errors, initial velocity errors, initial ψ-angle errors, bias east gyro drift, and bias north-axis accelerometer error.

At the conclusion of program checkout, a brief investigation was conducted using the error analysis program to determine the navigation errors induced by those error sources which are unique to the MICRON system. In particular, the effects of case-fixed gyro drift and scale factor ARO errors were studied for the MICRON system in the stationary laboratory environment.

For these studies, the RSA of the primary MESG was pointing up along the vertical and the RSA of the secondary MESG was pointing north. Thus, the RSA vectors in L-frame coordinates are:

$$\underline{\gamma}_1^{\,L} = \begin{bmatrix} 0 \\ 0 \\ -1 \end{bmatrix} \qquad \underline{\gamma}_2^{\,L} = \begin{bmatrix} 1 \\ 0 \\ 0 \end{bmatrix} \tag{3.3-7}$$

The attitude of the MICRON system was selected so that the center of the No. 1 electrode was parallel to the earth's axis of rotation (at the latitude of Anaheim, California) and that the x-axis of the M-frame was in the plane defined by the North and Down axes of the L-frame. Consequently, the transformation to the L-frame from the M-frame is:

$$C_M^L = \begin{bmatrix} 0.816 & -0.408 & -0.408 \\ 0 & -0.707 & 0.707 \\ -0.577 & -0.577 & -0.577 \end{bmatrix} \qquad (3.3\text{-}8)$$

Figure 3.3-2 presents the time history (for a 12-hr period) of the ψ-angles and the position and velocity errors for MICRON when the only error is a 0.005 deg/hr drift rate of the primary MESG about the x-case-fixed axis. Using Eq. (3.3-8), it can be seen that a drift rate about the x-case-fixed axis should cause drifts about the North and Down axes in the L-frame. The results in Fig. 3.3-2 show a ramping growth rate for ψ_N and ψ_Z which is the behavior that is expected due to constant gyro drift rates. The drift rates (through the interactions of the ψ-angle misalignments with the resolution of gravity) also lead to position and velocity errors which exhibit the anticipated behavior including Schuler and Foucault oscillations (Ref. 19). The apparent 42 min oscillation of the North velocity error is due to rectification of the negative portion of the Schuler oscillation occurring because covariance results are rms (and thus strictly positive) numbers.

The navigation errors induced by an x-axis scale factor ARO error for the primary MESG are presented in Fig. 3.3-3. As was derived in Section 3.2 and can be seen from the results, ARO errors do not drive the ψ-angle equations; rather, they cause velocity errors in the same manner as accelerometer misalignments. In a similar manner to the drift rate results, the apparent 42 min oscillation in the position and velocity errors is the classical Schuler dynamic behavior masked by the rectification due to the fact that the results are from covariance studies.

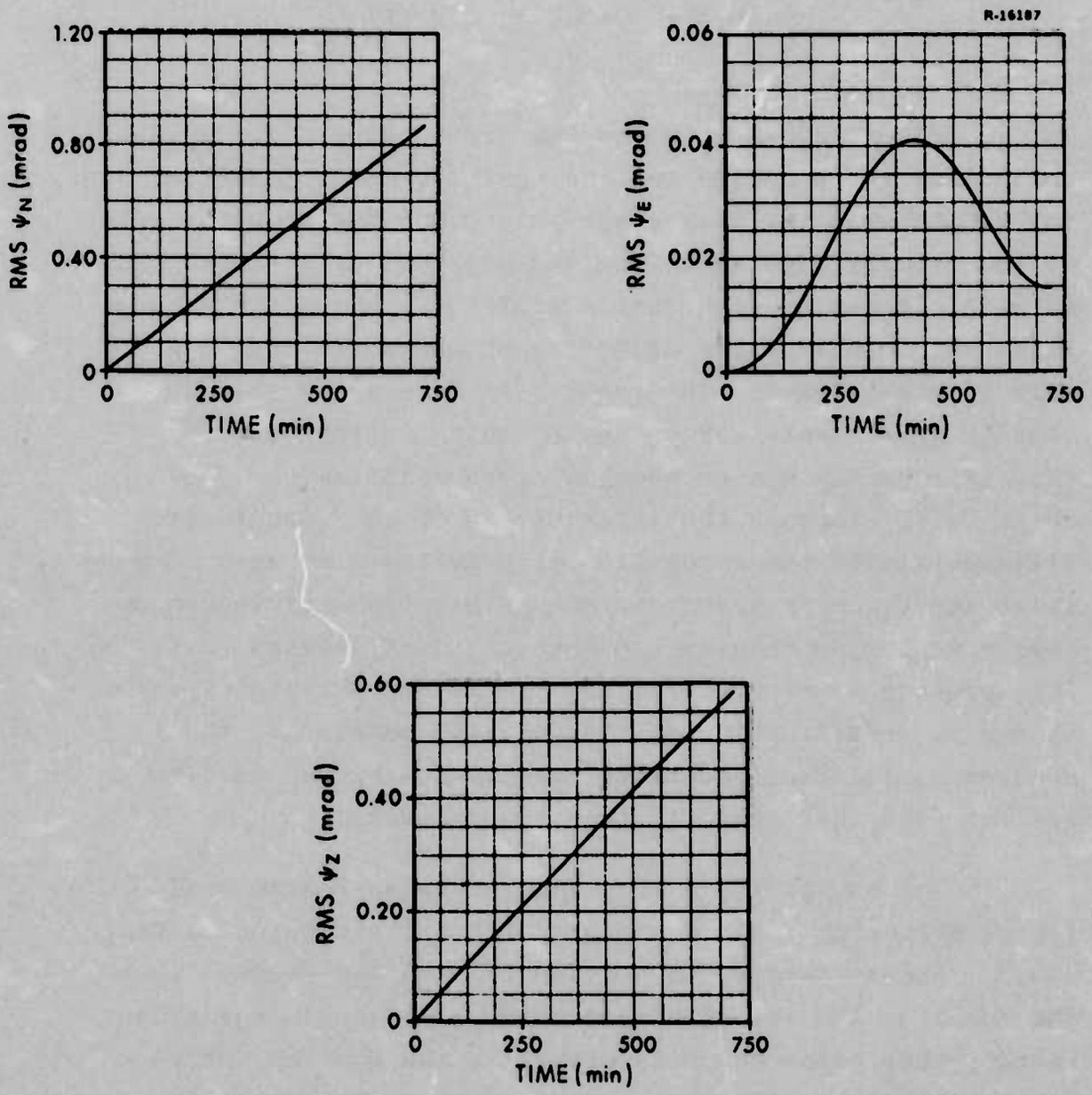

Figure 3.3-2 Navigation Errors Due to 0.005 deg/hr Drift of the Primary MESG About Case-Fixed x-Axis

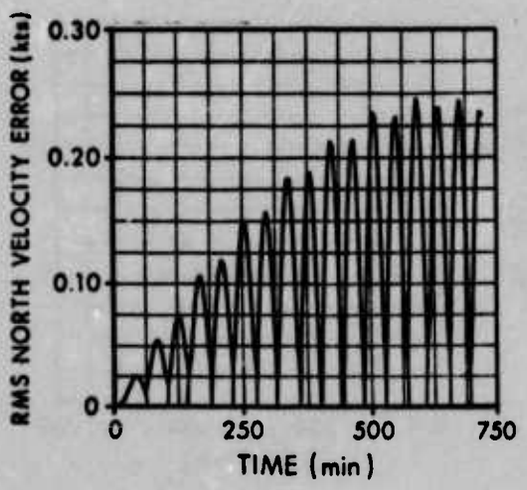

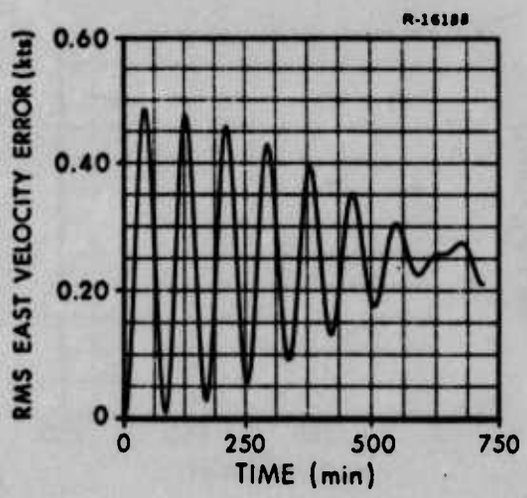

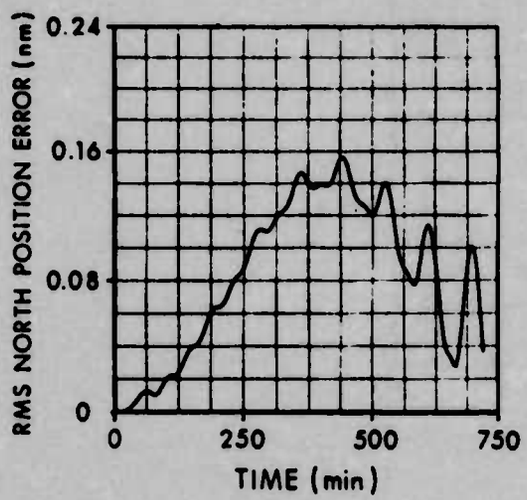

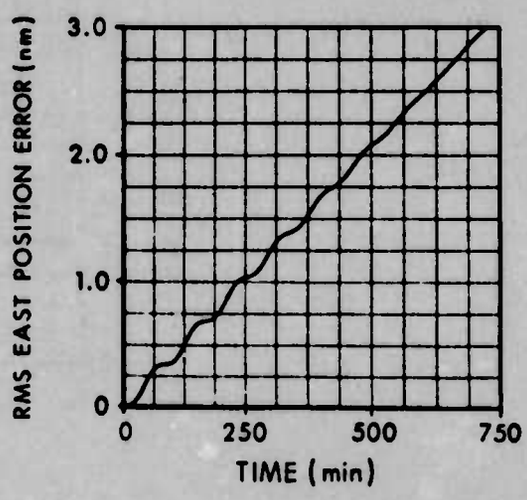

Figure 3.3-2 (Cont.) Navigation Errors Due to 0.005 deg/hr Drift of the Primary MESG About Case-Fixed x-Axis

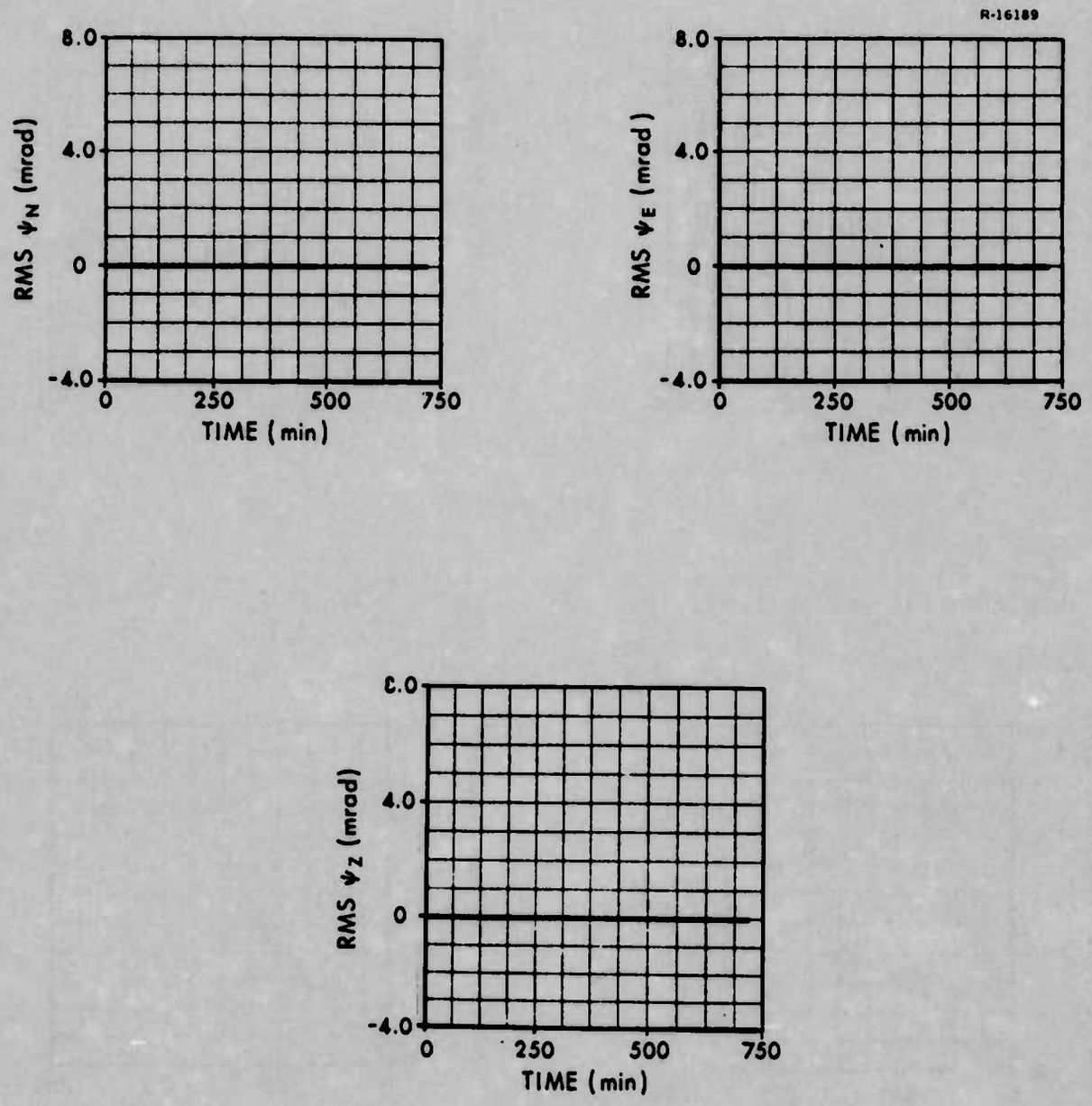

Figure 3.3-3 Navigation Errors Due to 0.1 mrad x-Scale Factor ARO Error in the Primary MESG

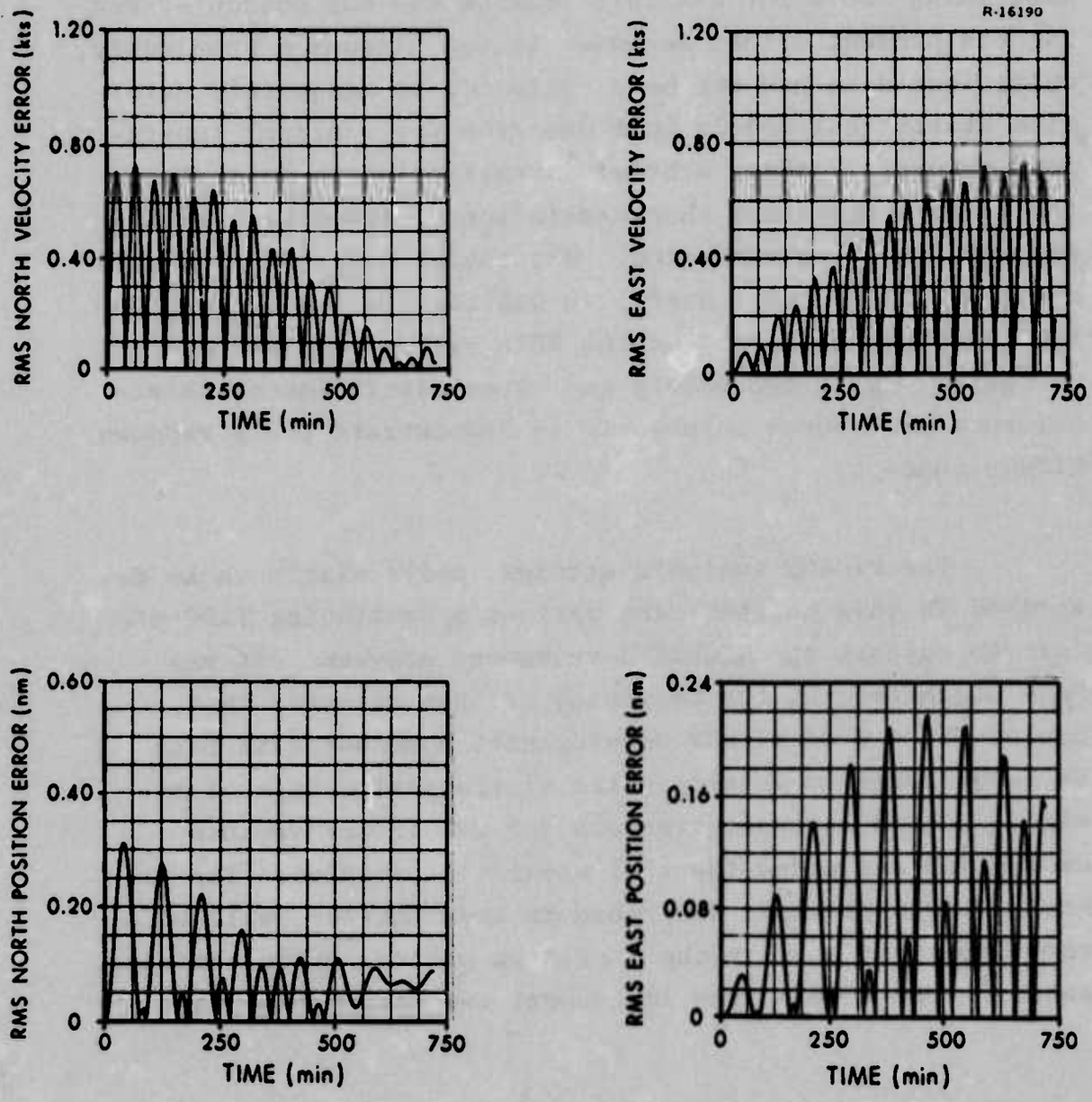

Figure 3.3-3 (Cont.) Navigation Errors Due to 0.1 mrad x-Scale Factor ARO Error in the Primary MESG

An exhaustive investigation of MICRON system performance using the error analysis program was not conducted during the present effort because, as was discussed previously, sufficient data has not been collected to adequately determine statistical models that describe the residual instrument errors. Rather, a brief investigation to determine the error propagation characteristics of the unique MICRON error sources was conducted. The insights gained from this study should be quite useful in qualitative evaluations of the test data collected on the N57A system (a developmental navigator, using two MESG's and three electro-magnetic accelerometers, whose purpose is to demonstrate the strapdown MICRON concept).

The MICRON analysis studies, particularly those described in this chapter, are part of a continuing TASC effort to support the MICRON development program. It has been suggested (at the beginning of this chapter) that, during Phase 2 of MICRON development, a sensor data bank be established to develop valid statistical models of residual MICRON instrument errors for use in performance evaluation and aided-inertial navigation studies. The error analysis program, described in this chapter, will be a very important tool in the iterative process of determining sensor error models from instrument and system test data.

4. TEST SUPPORT

In addition to exercising the MCSP and developing an error analysis program to statistically investigate MICRON performance, analytic support was provided to the N57A test program. The purpose of developing the N57A, which uses two MESG's as its orientation reference and three electromagnetic accelerometers (EMA's) to measure specific force, was to demonstrate the performance attainable with a strapdown MESG inertial navigator. The N57A was not designed to demonstrate MICRON's ultimate low cost and small size.

Section 4.1 will review the N57A Test Plan and discuss recommended improvements which resulted from this review. The results of the N57A tests conducted by Autonetics will be presented in Section 4.2 and observed performance will be compared with that delineated in the N57A specification. Section 4.3 will summarize the results and identify areas requiring additional development.

4.1 REVIEW OF THE N57A TEST PLAN

The goal of the N57A test program was to determine the system performance under both ambient and environmental conditions. Table 4.1-1 presents the performance targets for the N57A while Table 4.1-2 describes the environmental conditions which the system must withstand (Ref. 6). In addition to system level tests of the N57A, the Test Plan (Ref. 20) describes a complete sequence of module, subassembly and subsystem tests. The purpose of this testing was to verify the

TABLE 4.1-1

PERFORMANCE TARGETS FOR THE N57A

Horizontal Position Error	1 nm/hr, CEP (Least Squares, straight line fit)
Horizontal Velocity Error	5 ft/sec, time rms, per axis
Vertical Velocity Error	2 ft/sec, 1σ
Azimuth Error	4 $\widehat{\text{min}}$, 1σ
Roll, Pitch Errors	4 $\widehat{\text{min}}$, 1σ
Tilt Error	1 $\widehat{\text{min}}$, time rms, per axis
Reaction Time	1 hr from 0°F
Calibration Time	16 hrs
Calibration Stability	30 days

TABLE 4.1-2

ENVIRONMENTAL SPECIFICATIONS FOR THE N57A

Velocity Max	2000 ft/sec
Acceleration	9 g's
Shock	15 g, 11 ms, half sine wave
Vibration	MIL-E-5400M, Curve IVA
Angular Rate, Max	120 deg/sec
Angular Acceleration, Max	240 deg/sec^2
Operating Temperature Range	0 to 120°F
Altitude	0 to 15,000 ft
Nuclear	B-1 Level

integrity of the component functions at an intermediate level to reduce the problems associated with system integration.

The N57A system level tests begin during the last phase of system integration and continue through a lab test and a van test. Flight tests of the N57A, conducted by both Autonetics and the Central Inertial Guidance Test Facility (CIGTF) at Holloman AFB, are planned, following the van test program. Briefly summarized, the tests to be conducted during each phase are:

- System Integration Tests

  Align the N57A at a minimum of three headings and attitudes.

  Perform 4-hr navigation runs at a minimum of three different headings, changing heading and IMU tilt after two hrs during some of the runs.

- Lab Tests

  Four-hr navigation under Scorsby motion.

  The N57A will be exposed to environments including linear vibration, correlated angular and linear vibration, shock, and low temperature.

- Van Tests

  Align in the van at several headings.

  Perform 4-hr navigation runs using both triangular and constant heading courses.

The system integration and lab test phases of the test program are comprehensive and well-defined. In particular, the procedure which requires shakedown tests in each different environment, where the gyros are suspended but not spinning, prior to navigation tests in the environment is most prudent. This procedure will hopefully minimize the danger of secondary failure of the MESG. Successful completion of this test phase

should accomplish the dual objectives of evaluating N57A performance under the required conditions and qualifying the system for van testing.

Upon completing the review of the proposed lab test program, TASC made several suggestions concerning potential improvements to the proposed test sequence. Although Autonetics proposed a minimum testing philosophy with no redundant or unnecessary tests, it was suggested that static navigation runs be scheduled between each different set of environmental tests. The reason for these additional baseline navigation tests was to verify that the system was moved to the new test equipment properly and to ascertain that no permanent performance degradation had been induced by the previous environmental test. These tests will also generate more performance data on the N57A system.

The longest navigation test run that had been proposed by Autonetics was four hrs in duration. TASC suggested that at least one longer navigation test lasting 6-8 hrs be conducted during the lab tests. This longer duration navigation run should be used to demonstrate that there are no error sources peculiar to a MESG navigator that appear only after extended operation. (Eight hours was selected for the maximum duration of the navigation testing since that time interval will encompass most all mission applications for a moderate accuracy aircraft navigator). Also, a navigation test of this duration will allow preliminary investigation of the periodic long term error behavior associated with unaided inertial navigation (see Ref. 15 for a discussion of inertial system error dynamics).

The Test Plan published by Autonetics did not describe in great detail the van tests that were to be performed.

Following review of the proposed van tests, TASC suggested several improvements to the planned test procedures. These suggestions include:

- Conducting long duration (6 to 8 hr) van runs.
- Implementing an altimeter and an active vertical channel.
- Providing a velocity reference against which to evaluate N57A performance while the van is in motion.
- Defining a test course which has a significant variation in altitude (i.e., driving the test van into mountainous areas).

The reason for suggesting longer duration van runs are the same as those discussed for longer navigation tests in the lab. Including an altimeter and an active vertical channel in the van will allow checkout of these systems prior to moving the N57A into the flight test aircrafts. Providing a velocity reference permits velocity performance evaluation while the van is in motion which may facilitate identification of the causes of N57A navigation errors. Using a test course with significant altitude variations will enhance the van test program because it allows adequate exercising of the vertical channel and it induces an attitude change of the N57A during the steep climbs.

In summary, TASC has reviewed the N57A Test Plan and made comments and suggestions in areas of potential improvement. Many of the suggestions have been incorporated into the testing of the N57A conducted by Autonetics. In particular, all the suggested modifications of the van test program were to be incorporated into the second sequence of van tests conducted in March 1974.

4.2 N57A TEST RESULTS

The lab and van tests of the N57A system included 90 navigation runs under a large number of different conditions. The results of these tests presenting time history plots of position and velocity errors are contained in Refs. 21 and 22. Rather than reproducing all these results here, Table 4.2-1 presents a summary of the number of tests of each type that were conducted. This section will briefly discuss the results of each different environmental test and then comment on the performance of the N57A system during the entire test program.

TABLE 4.2-1

SUMMARY OF N57A LAB AND VAN TESTS

Type of Test	Number of Tests
Laboratory – Stationary	20
Laboratory – Stationary with Discrete Attitude Changes	12
Scorsby Motion	4
Linear Vibration	9*
Correlated Linear and Angular Vibration	3
Angular Rates	5
Shock	4**
Low Temperature	1
Van – Stationary	19
Van – Moving	17

*Four tests were conducted with the shaker field on, but with no vibration (see text)

**System was not operating during shock

4.2.1 Environmental Test Results

Since the performance goals are specified as ensemble statistics, relating N57A performance during the environmental tests to the performance targets presented in Table 4.1-1 is difficult because only a few tests were conducted in each environment. In a single test it is always possible to get a performance sample which is significantly worse than true average performance of the system. Only when a large number of samples (tests) are taken, can the results be viewed with confidence as a true indication of system performance. Because of this small sample size problem, the N57A environmental test results are discussed only qualitatively, pointing out potential performance problems that appear to be present in the few tests performed.

The results of the four Scorsby tests of the N57A that consist of four hours of navigation mode operation in the presence of continuous Scorsby motion indicate that this environment does not induce any significant errors. The performance of the N57A during the Scorsby testing is quite similar to performance obtained during stationary lab and van tests. Also, all four navigation runs during Scorsby motion have similar error magnitudes indicating that these samples are likely representative of the N57A performance during this motion and not anomalous results which can always occur in single trials with systems driven by stochastic error sources.

The performance of the N57A during the linear vibration tests was not as good as during the other environments. These vibrations, which consisted of sweeps between 2 and 10 g's in amplitude as the frequency was varied from 5 to 2000 Hz, caused particularly poor performance when they were applied along the vertical axis. Investigation of the test set up

led to the discovery that the shaker, which generated the vibration environment, produced a sizable magnetic field. This magnetic field caused a noticeable speed reduction of the MESG rotors when the vibration was applied along the vertical axis.

Attempting to separate the effects of the shaker's magnetic field from the vibration environment, navigation runs with the shaker field on but no vibrations were made in each test configuration. (Tests were made which applied vibrations along each of the vertical, lateral horizontal, and longitudinal horizontal axes.) These tests indicated that performance degradation occurred with and without the vibration as long as the shaker magnetic field was present. The performance degradation was most severe in the vertical vibration test set up. The N57A performance during the horizontal vibration test configuration did not appear to be affected very strongly by the shaker's field. Summarizing the linear vibration tests, N57A performance in this environment has not been clearly demonstrated due to disturbances induced by the test procedure, but it seems likely that a disturbance-free test environment would demonstrate satisfactory navigation performance in the presence of linear vibrations.

Neither the correlated linear and angular vibration tests, nor the shock tests identified any significant weakness in the N57A system performance. The results of correlated motion tests, which consisted of one test at each of three frequencies (64 Hz, 6.4 Hz, and the resonant frequency of the shock mounts), were all consistent with N57A performance goals. Although not unacceptably large, the worst errors (radial error rate = 1.49 nm/hr, rms velocity error = 2.995 fps) occurred during 64 Hz correlated motion. This frequency is the solution rate of the N57A fast cycle equations (Ref. 14) during which the accelerometers are sampled and projected on the inertial frame defined by the MESG spin axis attitude readouts. It would

be expected that correlated input motion at this frequency would be a source of error. The shock input of a 15g, 11 msec half sine wave was applied while the N57A was operating but without the MESG rotors spinning. This environment did not induce any system failures and no performance degradation was detected following the exposure to the shock environment.

The performance of the N57A at low temperature (0°F) was comparable to the other stationary lab test results. The reason for the low temperature test was to determine the reaction time of the system at 0°F. For this test the reaction time was 124 min (Ref. 23) which is twice the target of 60 min presented in Table 4.2-1. Reaction time is an area requiring significant improvement from the N57A to the MICRON system and is a task receiving considerable research and development effort from Autonetics (Ref. 24). Incorporation of automatic startup and heating should improve the system reaction time by eliminating the slow processes of manual polhode damping and rotor heating.

The angular rate testing included one run with three hours of continuous 12°/sec yaw rate and three one-hour tests with short duration (only long enough to get the test table up to the desired speed and stopped again) high rate inputs at 30 min. The high rate inputs were 40°/sec in yaw, 300°/sec in roll, and 100°/sec in pitch. The angular rate inputs did not appear to cause any significant degradation of N57A navigation accuracy. In summary, the N57A accuracy does not appear to be reduced by Scorsby motion, correlated linear and angular vibration, shock, low temperature or high angular rates. The observed performance degradation in the presence of linear vibration is likely due to the test set up and not to the vibration input but a modified test configuration would be needed to verify the vibration performance. The reaction time of the N57A from low temperature did not meet the goal, indicating that additional effort is required in this area.

4.2.2 N57A Performance Evaluation

To quantitatively estimate the N57A system performance from the lab and van test results, all 90 navigation runs were considered to provide a data base large enough to be statistically significant. Figures 4.2-1 and 4.2-2 summarize on histograms the radial error rate and time rms velocity error results observed by Autonetics during the test program. Different symbols are used in the figures to distinguish stationary lab tests, lab environmental tests, stationary van tests and moving van tests.

The horizontal position error growth rate performance target for the N57A is 1 nm/hr CEP (least squares straight line fit to radial error) which means that, on the average, 50% of the time the observed radial error rate will be less than 1 nm/hr. The estimate of the position error performance of the N57A was computed by tabulating the computed slopes of a least squares straight line fit to the radial position error time histories for the test results and selecting the median value. This method yielded a value of 0.87 nm/hr as the CEP rate for the N57A.

The N57A performance target for velocity accuracy is a 1σ value of 5 ft/sec, time rms per axis. A 1σ performance number implies that, on the average, 68% of the time the system accuracy will equal or better the specified value. The 68 percentile velocity error performance was computed, in a similar manner to the position computation, to be 3.15 ft/sec.

Measurement of the attitude errors of the N57A during a navigation run, particularly when motion is involved, is difficult to accomplish due to problems in defining a reference against which N57A outputs can be compared. Consequently, very little attitude accuracy data was collected during the

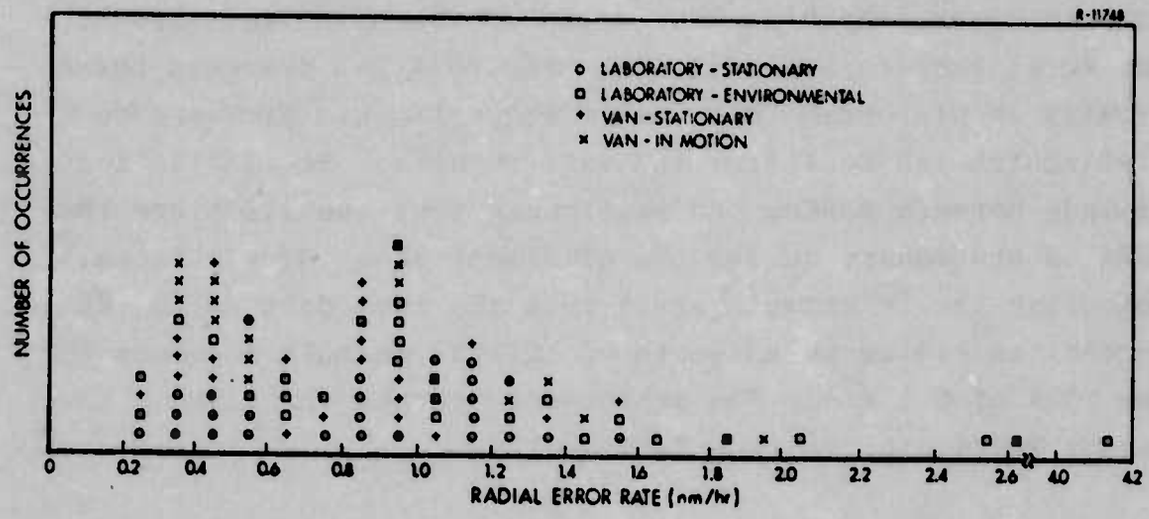

Figure 4.2-1 N57A Position Error Histogram
(Data Provided by Autonetics)

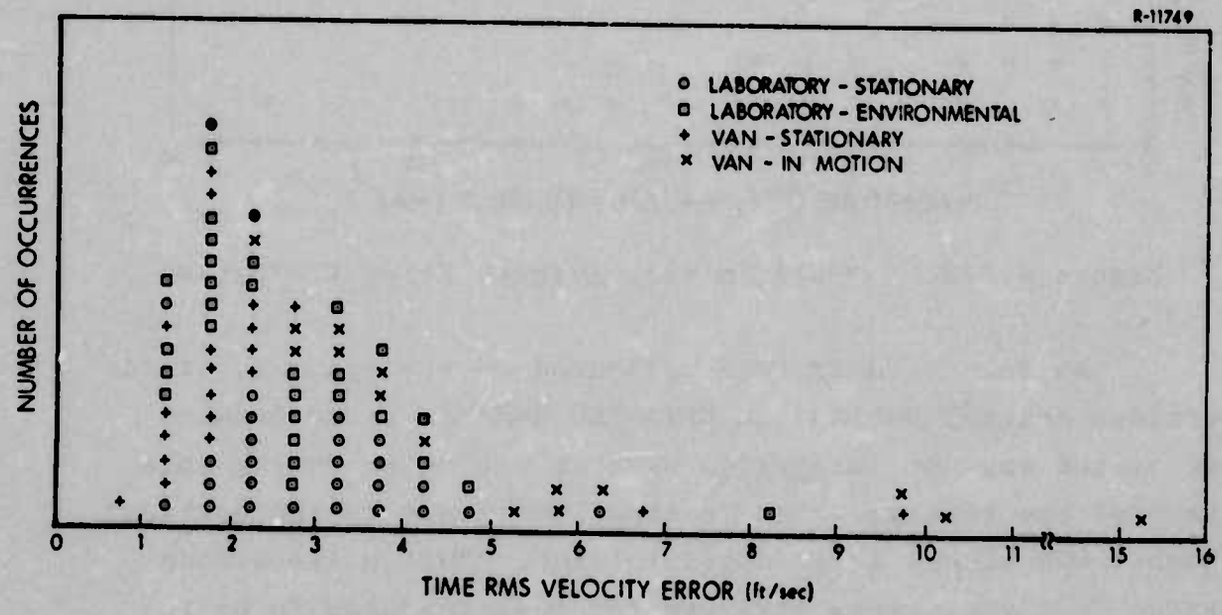

Figure 4.2-2 N57A Velocity Error Histogram
(Data Provided by Autonetics)

test program. For about one-third of the tests, the initial azimuth error, which is indicative of system performance during alignment, was measured. Figure 4.2-3 presents these results in histogram form. (Different symbols are used to distinguish lab test from van test results. No distinction is made between moving and stationary test results since the N57A is stationary during the alignment phase of all tests.) Computing the 1σ azimuth error from the test data as the 68 percentile yields an estimate of initial azimuth accuracy for the N57A of 6.1 $\widehat{\text{min}}$. The performance target for azimuth accuracy was 4 $\widehat{\text{min}}$, 1σ (see Table 4.1-1).

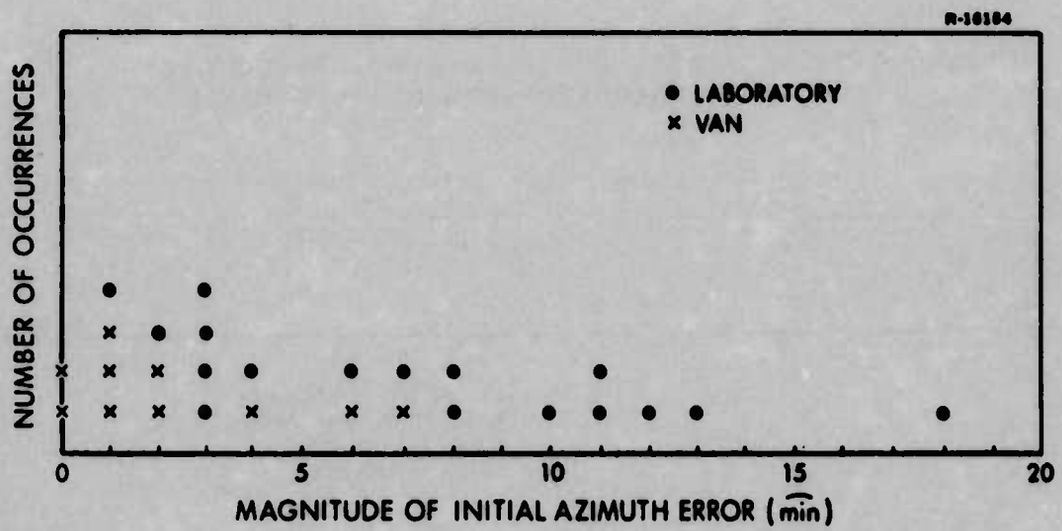

Figure 4.2-3 N57A Initial Azimuth Error Histogram

No test results were collected on the accuracy of the vertical channel during the N57A lab and van tests because the system was not integrated with an altimeter during this phase of the test program. Rather, the input to the vertical channel was pinned at a constant value. During the second set of N57A van tests, an altimeter was scheduled to be included and the vertical performance of the N57A was to be evaluated. Prior to the beginning of these tests, the N57A

was modified to incorporate completely automatic startup capability. This modification induced a hardware problem (the MESG feed-through pins became magnetized during startup) which prevented any useful performance data from being collected during these van tests. It was possible to check out the altimeter interface, but evaluation of the vertical channel performance was postponed until the flight tests.

Evaluation of the stability of the N57A calibration parameters during the test program is difficult because hardware problems prevented extended operation of the system between calibrations. Table 4.2-2 presents the calibration history of the N57A including the reason for each recalibration and the number of tests performed in the interval. The heading sensitivity which precipitated the recalibration following Test No. 29 was isolated to a calibration parameter shift. All the other recalibrations made during the lab and van testing were due to causes other than calibration parameter shifts. Thus, the one sample that is indicative of N57A calibration stability is 28 days. (The target for calibration stability was 30 days.) Additional testing will

TABLE 4.2-2

CALIBRATION STABILITY RESULTS

CALIBRATION DATE (Approximate)	SYSTEM OPERATION		REASON FOR RECALIBRATION	TIME BETWEEN CALIBRATIONS (Days)
	Dates	Test Numbers		
8/10/73	8/10/73 - 9/ 7/73	1-29	System developed heading sensitivity	28
9/14/73	9/14/73 - 9/25/73	30-47K	Failed hardware in system	12
10/24/73	10/24/73 - 10/26/73	48-52	System failed following cold soak	2
11/ 9/73	11/ 9/73 - 11/27/73	53-71	Test sequence completed	18
1/24/74	1/24/74 - 1/25/74	72-80	Automatic startup problems	1

clearly be required to develop confidence that the stability of the MESG compensation parameters is adequate to achieve the desired calibration intervals.

4.3 TEST SUPPORT SUMMARY AND CONCLUSIONS

In support of the N57A test program, TASC has reviewed the proposed system level lab and van test plans and made recommendations concerning potential improvements to the planned tests and procedures. Several of these suggestions which included baseline navigation runs between environmental tests, longer duration navigation runs, and incorporation of an altimeter and a velocity reference in the mobile test vehicle were adopted by Autonetics for portions of the test program.

The results of the N57A lab and van tests were evaluated to determine the system performance. This performance may be summarized as

- Radial Error Rate CEP = 0.87 nm/hr
- Horizontal Velocity Error, 1σ = 3.2 ft/sec
- Initial Azimuth Error, 1σ = 6.1 $\hat{\text{min}}$
- Reaction Time from 0°F = 124 min
- Calibration Stability $\leq$ 28 days

The N57A system accuracy during the test program compares reasonably well with the performance targets presented in Table 4.1-1. Those areas which the test program has identified as needing additional testing and development are reaction time and calibration stability. Also, flight test performance still must be demonstrated. There are some system level error sources which will be more visibly excited by the high acceleration and velocity environments of an aircraft [in particular, the ($\underline{\psi}$ x $\underline{f}$) term in Eq. (3.2-2)].

Thus, it may be anticipated that larger navigation errors will be observed during the flight tests than were seen during lab and van testing.

Comparing the observed N57A performance with the error budget developed for this system early in the MICRON Program points out a conflicting set of circumstances. While the N57A navigation accuracy was generally better than the target, the MESG drift rate and attitude readout residuals were larger than allowed by the error budget. This discrepancy is likely due to the use of improper statistical models for the MESG error residuals in generating the error budget. Because of the high order of the MESG compensation models, the error residuals are likely of high harmonic order in case-rotor orientation. Consequently, the vibration environment to which a strapdown navigator is exposed may reduce the effective residual errors by "dithering" the RSA vector in case coordinates. It is suggested that future studies be undertaken to attempt to determine valid statistical models for the MESG error residuals. These models are required not only for reconciliation of the MICRON error budget but also for development of Kalman filtering techniques for integrating MICRON with various navaids such as doppler radar, OMEGA, and navigation satellites.

Summarizing, the N57A lab and van tests have accomplished the goal of demonstrating 1 nm/hr navigation accuracy using MESG's in a strapdown mode. The environmental testing conducted tends to indicate the navigation accuracy is not significantly degraded by exposure to the test environments. (Linear vibration resistance requires further demonstration due to test equipment induced magnetic fields.) Further testing is planned to demonstrate the performance of the N57A in both fighter and transport aircraft and helicopters. Based on the results of the lab and van tests, the two-hour

reaction time in a low temperature environment and the calibration stability are the performance areas requiring greatest improvement to develop an inertial navigation system suitable for operational deployment.

5. SUMMARY AND CONCLUSIONS

The results of three closely related system-level analyses conducted by TASC in support of the MICRON development program have been presented. These studies consisted of:

- Exercising the previously developed MICRON Computer Simulation Program (MCSP) to evaluate the effects of MESG instrument variations and severe environments on navigation performance.
- Developing models to describe the propagation of instrument errors into navigation system errors and generating a covariance analysis computer program to conduct statistical performance predictions for MICRON.
- Supporting the test program of the N57A demonstration system by reviewing the Test Plan developed by Autonetics and by evaluating the laboratory and van test data.

The MCSP studies investigated the effects on MICRON performance of reducing the preload charge level on the MESG's, eliminating the instrument turn-on repeatability errors, and subjecting the system to high vibration and roll rate environments. A 15% performance improvement was observed in the simulation results when the preload charge level was reduced by 30%. Comparable performance improvement was also predicted by the MCSP studies when only the MESG calibration errors (gyro turn-on repeatability errors were eliminated) were used to drive the system. The MCSP results indicated that neither high vibration nor high roll rate and acceleration environments should prevent the MICRON system from achieving its specified navigation accuracy.

A covariance analysis computer program (to be used for statistical error propagation studies) was developed to supplement the MCSP and to increase the capability to simulate MICRON system performance. The derivation of the MICRON error equations has been presented, the structure of the covariance analysis program has been described, and the results of a brief investigation to determine the propagation characteristics of those error sources unique to MICRON have been discussed. Because there is insufficient data available to allow development of valid statistical models describing residual MESG errors, it was assumed during the present studies that the errors were due to miscalibration of several of the drift rate and ARO error compensation coefficients.

It is strongly suggested that development of models to describe the residual MESG errors be given high priority during future MICRON Analysis studies since these models of the MICRON system are needed for use in modern data processing algorithms (e.g., Kalman filtering) which will combine MICRON data with the navaids that are available in a modern avionics suite. To aid in this effort, it was suggested that a sensor data bank in which to store data collected on all MESG's that are manufactured be established. Residual error model determination is an iterative process during which test data is analyzed, models are postulated, and model predicted system performance is compared with test data. The covariance analysis program developed in this report will be a very useful tool in this effort.

In support of the N57A test program, TASC reviewed the Test Plan document and evaluated the test data collected. The review of the Test Plan suggested several areas where improvement could be made. In particular, with respect to the van test program, the following suggestions were made:

- Conduct long duration (6 to 8 hr) van runs.
- Implement an altimeter and an active vertical channel.
- Provide a velocity reference in the van against which to evaluate N57A performance.
- Include significant altitude variations in the van test courses.

Many of these suggestions were adopted by Autonetics for the second set of van tests planned for the N57A.

Evaluation of the data collected during the N57A laboratory, environmental, and van test programs indicates that the observed system performance achieves most of the targets that were established for the system. The computed system accuracy based on all the tests performed was

- Radial error rate CEP = 0.87 nm/hr
- Horizontal velocity error (1σ) = 3.2 ft/sec

None of the environments to which the N57A was subjected identified any significant performance deficiency, although vibration performance has not been completely verified due to test equipment problems. Those areas which have been identified by the results of the test program as requiring additional testing and development are reaction time and calibration stability.

A reevaluation of the MICRON design error budget should be conducted in light of the results of the N57A test program. Due to the lack of valid models to describe residual MESG errors, the design error budget apparently imposed unnecessarily severe specifications on MESG residual errors. (Although the observed system performance was consistent with the targets, the residual instrument errors

were generally larger than the values allowed in the error budget.) Additional analytic effort will be required to resolve this issue and define a revised error budget for the final MICRON design.

APPENDIX A

ERROR EQUATIONS FOR MICRON'S VERTICAL CHANNEL DAMPING

The vertical channel damping of the MICRON system is implemented by using an altimeter to generate a vertical position error signal which is fed back to the input of the vertical velocity and position integrators. The altimeter output is not used in the gravity calculation. Viewing the vertical channel as uncoupled, Fig. A-1 represents the mechanization of the vertical channel for MICRON (this corresponds to the $\kappa = 0$ case discussed in Ref. 26). The gains k_1 and k_2 in Fig. A-1 are, for the MICRON system,

$$k_1 = 2/\tau \tag{A-1}$$

$$k_2 = 2\omega_s^2 + \frac{1}{\tau^2 \xi^2} \tag{A-2}$$

where $\tau = 100$ sec and $\xi = 0.7$ (Ref. 21).

As derived in Ref. 26, the error diagram that corresponds to the MICRON vertical channel mechanization is presented in Fig. A-2. From this error diagram, it is possible to write the uncoupled vertical channel error equations as

$$\dot{\delta r}_D = \delta v_D - k_1(\delta r_D + \delta h_R) \tag{A-3}$$

$$\dot{\delta v}_D = \delta f_D + 2\omega_s^2 \, \delta r_D - k_2(\delta r_D + \delta h_R) \tag{A-4}$$

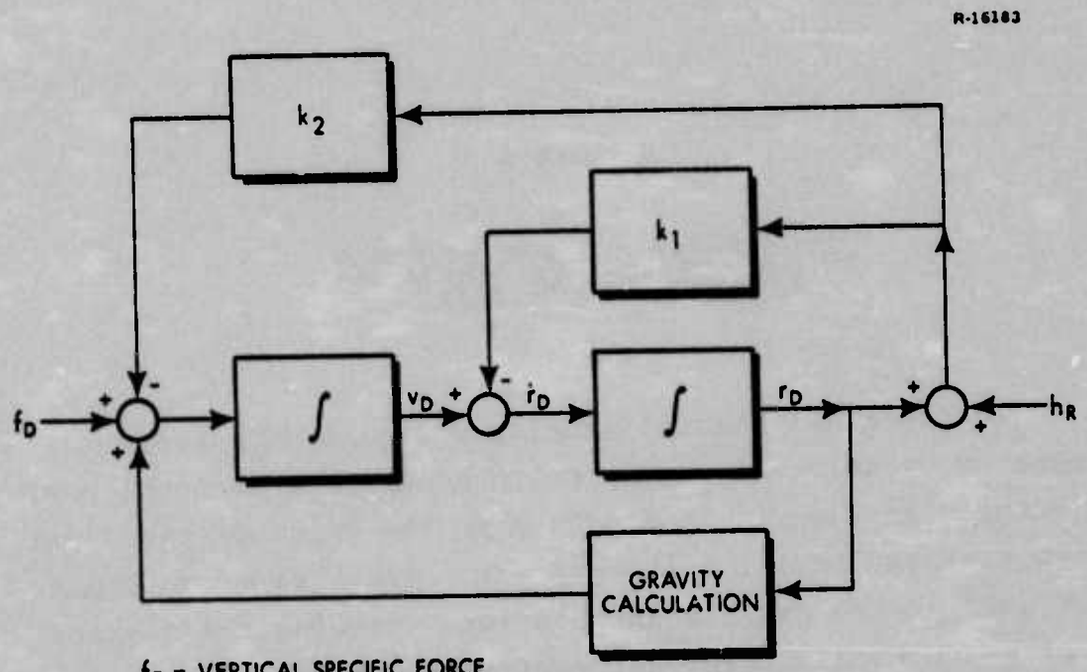

f_D - VERTICAL SPECIFIC FORCE
v_D - VERTICAL VELOCITY
r_D - VERTICAL POSITION (POSITIVE DOWN)
h_R - ALTIMETER OUTPUT (POSITIVE UP)

Figure A-1 Vertical Channel Mechanization for the MICRON System

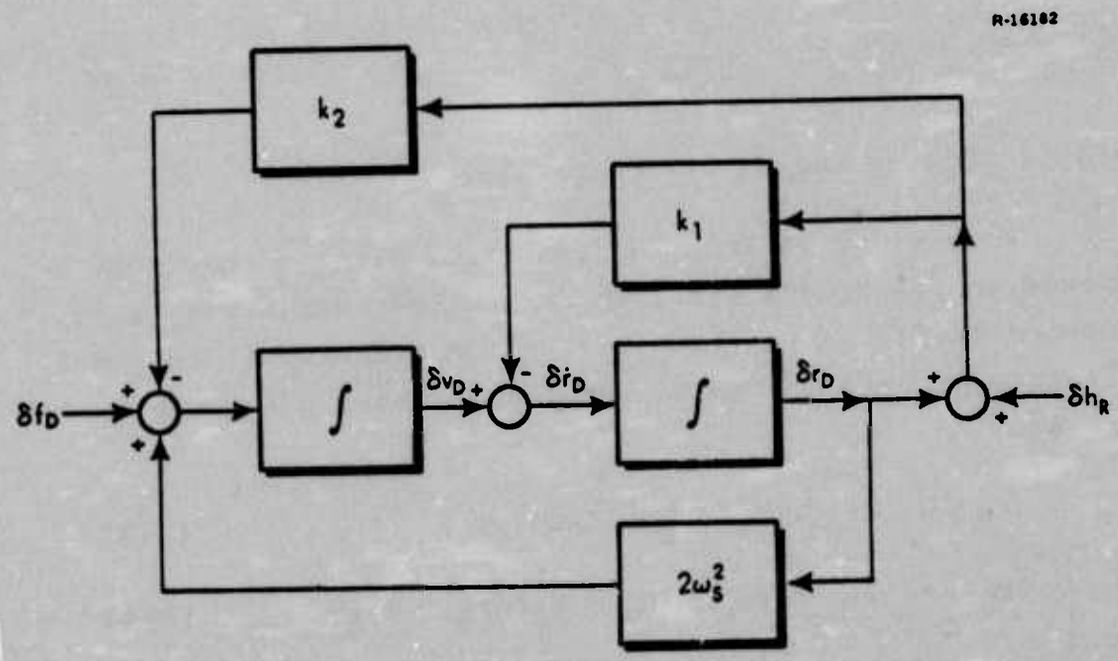

Figure A-2 MICRON Altitude Channel Error Diagram

The altimeter output and vertical position are defined with their positive directions being opposite (altimeter output is positive up, while vertical position is positive down in a NED frame) which accounts for the sum ($\delta r_D + \delta h_R$) being fed back in the error equations.

The term δf_D in Eq. (A-4) is the third element of $\delta \underline{f}^L$ defined in Eq. (3.2-12) and includes effects of both the accelerometer and ARO errors that excite the vertical channel. Equations (A-3) and (A-4), with the inclusion of the coupling terms, are the equations that model the vertical channel in the error analysis computer program. Appendix B contains a complete listing of the state vector and system dynamics matrix that describe the MICRON navigation performance.

APPENDIX B

MODEL DEFINITION FOR ERROR ANALYSIS COMPUTER PROGRAM

This appendix presents the state vector and dynamics matrix implemented in the covariance error analysis computer program. In Chapter 3, the MICRON error equations were derived in vector-matrix form and the models describing the residual instrument errors that drive the error equations were selected. Table 3.3-1 indicates that, in addition to the 9 system states, 33 error sources were included in the MICRON system error model. A vector of 45 states is required to represent the MICRON navigation performance in a stationary, laboratory environment.

Table B-1 defines the elements of this state vector which is the basis of the error analysis computer program. Since it was decided to perform the error analysis in the local-level, north-east-down L-frame, all the elements of the system state vector are coordinatized in this frame. The describing parameters of those instrument errors which occur in the gyro case fixed M-frame (case fixed bias drift rates, accelerometer errors, and scale factor ARO errors) are input relative to this frame and transformed by the error analysis program initialization module to generate equivalent errors in the L-frame.

For the stationary, laboratory environment, the gravity vector is always along the down-axis of the L-frame. This fact has been used to reduce the number of states required to model the MICRON system (for example, only the

TABLE B-1

STATE VECTOR FOR ERROR ANALYSIS PROGRAM

$x_1 = \psi_N$
$x_2 = \psi_E$
$x_3 = \psi_Z$
} misalignments

$x_4 = \delta v_N$
$x_5 = \delta v_E$
$x_6 = \delta v_D$
} navigator velocity error

$x_7 = \delta r_N$
$x_8 = \delta r_E$
$x_9 = \delta r_D$
} navigator position error

$x_{10} = \delta C_{1D}\, \gamma_{1N}$
$x_{11} = \delta C_{1D}\, \gamma_{1E}$
$x_{12} = \delta C_{1D}\, \gamma_{1D}$
$x_{13} = \delta C_{2D}\, \gamma_{2N}$
$x_{14} = \delta C_{2D}\, \gamma_{2E}$
$x_{15} = \delta C_{2D}\, \gamma_{2D}$
$x_{16} = \delta C_{NE}\, \gamma_{1N}\, \gamma_{2N}$
$x_{17} = \delta C_{NE}\, \gamma_{1N}\, \gamma_{2E}$
$x_{18} = \delta C_{NE}\, \gamma_{1N}\, \gamma_{2D}$
$x_{19} = \delta C_{NE}\, \gamma_{1E}\, \gamma_{2N}$
$x_{20} = \delta C_{NE}\, \gamma_{1E}\, \gamma_{2E}$
$x_{21} = \delta C_{NE}\, \gamma_{1E}\, \gamma_{2D}$
$x_{22} = \delta C_{NE}\, \gamma_{1D}\, \gamma_{2N}$
$x_{23} = \delta C_{NE}\, \gamma_{1D}\, \gamma_{2E}$
$x_{24} = \delta C_{NE}\, \gamma_{1D}\, \gamma_{2D}$
} Attitude Readout Scale Factor Error States

Note: $\delta C_{NE} = \delta C_{1N} + \delta C_{2E}$
$= \delta C_{1E} + \delta C_{2N}$

$x_{25} = \delta P_C\, \gamma_{1N}\, \gamma_{1N}$
$x_{26} = \delta P_C\, \gamma_{1N}\, \gamma_{1E}$
$x_{27} = \delta P_C\, \gamma_{1N}\, \gamma_{1D}$
$x_{28} = \delta P_C\, \gamma_{1E}\, \gamma_{1E}$
$x_{29} = \delta P_C\, \gamma_{1E}\, \gamma_{1D}$
$x_{30} = \delta P_C\, \gamma_{1D}\, \gamma_{1D}$
} γ-dependent propagation of bias drift rate errors

Note: $\delta P_C = c_{B1N} - c_{B2N}$
$= c_{B1E} - c_{B2E}$
$= c_{B1D} - c_{B2D}$

$x_{31} = \nabla_{rN}$
$x_{32} = \nabla_{rE}$
$x_{33} = \nabla_{rD}$
} random accelerometer errors

$x_{34} = c_{rN}$
$x_{35} = c_{rE}$
$x_{36} = c_{rD}$
} random drift rate errors

$x_{37} = \delta h_R$ – altimeter error

$x_{38} = c_{B1N}$
$x_{39} = c_{B1E}$
$x_{40} = c_{B1D}$
} bias drift rate error for MESG No. 1

$x_{41} = \delta P_g$ – error in axial mass unbalance coefficiant

$x_{42} = \nabla_{bN}$
$x_{43} = \nabla_{bE}$
$x_{44} = \nabla_{bD}$
} bias accelerometer errors

$x_{45} = \delta C_{safD}$ – "vertical" accelerometer scale factor error

"vertical" accelerometer scale factor is required). Since drift rate and ARO errors propagate into MICRON navigation errors as functions of the RSA direction vectors (see Section 3.2), a large number of states are required to properly model these effects. Although the error terms in these cases (case fixed drift rate or ARO scale factor error) have no dynamics, the states required in the model are governed by the dynamics of the RSA vectors. For the present study, the motion of the RSA vectors relative to the L-frame is due solely to earth rate.

Figure B-1 presents the F matrix which describes the dynamics of all the states appearing in the error analysis computer program. Table B-2 defines the parameters which appear in the F matrix. To complete the specification of those matrices necessary to propagate the covariance matrix in the error analysis program, it is necessary to define the continuous noise matrix Q that appears in Eq. (3.3-5). The only elements of the Q matrix which are non-zero are the diagonal elements corresponding to the random drift rate and accelerometer errors. For these states, which are modeled as first order Markov processes, the value entered in the Q matrix is $2\sigma^2\beta$ where $1/\beta$ is the correlation time of the process and σ is the rms value of the error.

Because many of the states in the MICRON system error vector model the equivalent effects in the L-frame of errors which actually occur in the gyro case fixed M-frame, the initialization of the covariance matrix, P, defined as

$$P = E\left[\underline{x}\,\underline{x}^T\right] \qquad \text{(B-1)}$$

is not as simple as for classical inertial system error analyses. Typically, the system error sources are assumed to be statistically independent resulting in an inertial covariance matrix that is diagonal. In the MICRON system analysis,

MISALIGNMENTS	NAVIGATOR VELOCITY ERROR	NAVIGATOR POSITION ERROR	ATTITUDE READOUT SCALE FACTOR ERROR STATES	Y-DEPENDENT PROPAGATION OF BIAS DRIFT RATE ERRORS	RANDOM ACCELEROMETER ERRORS	
$\begin{matrix} 0 & \Omega_D & 0 \\ -\Omega_D & 0 & \Omega_N \\ 0 & -\Omega_N & 0 \end{matrix}$	0	0	F_1	$\begin{matrix} 1 & 1 & 1 & 0 & 0 & 0 \\ 0 & 1 & 0 & 1 & 1 & 0 \\ 0 & 0 & 1 & 0 & 1 & 1 \end{matrix}$	$\begin{matrix} -P_E & 0 & 0 \\ 0 & -P_E & 0 \\ 0 & 0 & -P_E \end{matrix}$	
$\begin{matrix} 0 & g & 0 \\ -g & 0 & 0 \\ 0 & 0 & 0 \end{matrix}$	$\begin{matrix} 0 & 2\Omega_D & 0 \\ -2\Omega_D & 0 & 2\Omega_N \\ 0 & -2\Omega_N & 0 \end{matrix}$	$\begin{matrix} -\frac{k}{R} & 0 & 0 \\ 0 & -\frac{k}{R} & 0 \\ 0 & 0 & 2\frac{k}{R} - k_2 \end{matrix}$	F_2	0	$\begin{matrix} 1 & 0 & 0 \\ 0 & 1 & 0 \\ 0 & 0 & 1 \end{matrix}$	
0	$\begin{matrix} 1 & 0 & 0 \\ 0 & 1 & 0 \\ 0 & 0 & 1 \end{matrix}$	$\begin{matrix} 0 & 0 & 0 \\ 0 & 0 & 0 \\ 0 & 0 & -k_1 \end{matrix}$	0	0	0	
0	0	0	F_3	0	0	
0	0	0	0	$\begin{matrix} 0 & 2\Omega_D & 0 & 0 & 0 & 0 \\ -\Omega_D & 0 & \Omega_N & \Omega_D & 0 & 0 \\ 0 & -\Omega_N & 0 & 0 & \Omega_D & 0 \\ 0 & -2\Omega_D & 0 & 0 & 2\Omega_N & 0 \\ 0 & 0 & -\Omega_D & -\Omega_N & 0 & \Omega_N \\ 0 & 0 & 0 & 0 & -2\Omega_N & 0 \end{matrix}$	0	
0	0	0	0	0	$\begin{matrix} -\beta_{VN} & 0 & 0 \\ 0 & -\beta_{VE} & 0 \\ 0 & 0 & -\beta_{VD} \end{matrix}$	
0	0	0	0	0	0	
0	0	0	0	0	0	
0	0	0	0	0	0	
0	0	0	0	0	0	
0	0	0	0	0	0	
0	0	0	0	0	0	

Figure B-1 F-Matrix for Error Analy

Y-DEPENDENT PROPAGATION OF BIAS DRIFT RATE ERRORS	RANDOM ACCELEROMETER ERRORS	RANDOM DRIFT RATE ERRORS	ALTIMETER ERROR	BIAS DRIFT RATE ERROR FOR MSSG NO. 1	ERROR IF AXIAL MASS UNBALANCE COEFFICIENT	BIAS ACCELEROMETER ERRORS	"VERTICAL" ACCELEROMETER SCALE FACTOR ERROR
$\begin{matrix}1&1&1&0&0&0\\0&1&0&1&1&0\\0&0&1&0&1&1\end{matrix}$	$\begin{matrix}-P_g&0&0\\0&-P_g&0\\0&0&-P_g\end{matrix}$	$\begin{matrix}1&0&0\\0&1&0\\0&0&1\end{matrix}$	0	$\begin{matrix}1&0&0\\0&1&0\\0&0&1\end{matrix}$	$\begin{matrix}0\\0\\-g\end{matrix}$	$\begin{matrix}-P_g&0&0\\0&-P_g&0\\0&0&-P_g\end{matrix}$	$\begin{matrix}0\\0\\-P_g\,g\end{matrix}$
0	$\begin{matrix}1&0&0\\0&1&0\\0&0&1\end{matrix}$	0	$\begin{matrix}0\\0\\-k_2\end{matrix}$	0	0	$\begin{matrix}1&0&0\\0&1&0\\0&0&1\end{matrix}$	$\begin{matrix}0\\0\\g\end{matrix}$
0	0	0	$\begin{matrix}0\\0\\-k_1\end{matrix}$	0	0	0	0
0	0	0	0	0	0	0	0
$\begin{matrix}0&2\Omega_D&0&0&0&0\\-\Omega_D&0&\Omega_N&\Omega_D&0&0\\0&-\Omega_N&0&0&\Omega_D&0\\0&-2\Omega_D&0&0&2\Omega_N&0\\0&0&-\Omega_D&-\Omega_N&0&\Omega_N\\0&0&0&0&-2\Omega_N&0\end{matrix}$	0	0	0	0	0	0	0
0	$\begin{matrix}-\beta_{VN}&0&0\\0&-\beta_{VE}&0\\0&0&-\beta_{VD}\end{matrix}$	0	0	0	0	0	0
0	0	$\begin{matrix}-\beta_{cN}&0&0\\0&-\beta_{cE}&0\\0&0&-\beta_{cD}\end{matrix}$	0	0	0	0	0
0	0	0	0	0	0	0	0
0	0	0	0	0	0	0	0
0	0	0	0	0	0	0	0
0	0	0	0	0	0	0	0
0	0	0	0	0	0	0	0

Figure B-1 F-Matrix for Error Analysis Program

TABLE B-2

PARAMETERS USED IN FIGURE B-1

$$F_1 = \begin{bmatrix} 0 & 0 & -P_g u_{xN}^g & 0 & 0 & -P_g u_{yN}^g & 0 & -P_g u_{zN}^g & 0 & P_g u_{zN}^g & 0 & 0 & 0 & 0 & 0 \\ 0 & 0 & -P_g u_{xE}^g & 0 & 0 & -P_g u_{yE}^g & 0 & -P_g u_{zE}^g & 0 & P_g u_{zE}^g & 0 & 0 & 0 & 0 & 0 \\ 0 & 0 & -P_g u_{xD}^g & 0 & 0 & -P_g u_{yD}^g & 0 & -P_g u_{zD}^g & 0 & P_g u_{zD}^g & 0 & 0 & 0 & 0 & 0 \end{bmatrix}$$

$$F_2 = \begin{bmatrix} 0 & 0 & u_{xN}^g & 0 & 0 & u_{yN}^g & 0 & u_{zN}^g & 0 & -u_{zN}^g & 0 & 0 & 0 & 0 & 0 \\ 0 & 0 & u_{xE}^g & 0 & 0 & u_{yE}^g & 0 & u_{zE}^g & 0 & -u_{zE}^g & 0 & 0 & 0 & 0 & 0 \\ 0 & 0 & u_{xD}^g & 0 & 0 & u_{yD}^g & 0 & u_{zD}^g & 0 & -u_{zD}^g & 0 & 0 & 0 & 0 & 0 \end{bmatrix}$$

$$F_3 = \begin{bmatrix} 0 & \Omega_D & 0 & 0 & 0 & 0 & 0 & 0 & 0 & 0 & 0 & 0 & 0 & 0 & 0 \\ -\Omega_D & 0 & \Omega_N & 0 & 0 & 0 & 0 & 0 & 0 & 0 & 0 & 0 & 0 & 0 & 0 \\ 0 & -\Omega_N & 0 & 0 & 0 & 0 & 0 & 0 & 0 & 0 & 0 & 0 & 0 & 0 & 0 \\ 0 & 0 & 0 & 0 & \Omega_D & 0 & 0 & 0 & 0 & 0 & 0 & 0 & 0 & 0 & 0 \\ 0 & 0 & 0 & -\Omega_D & 0 & \Omega_N & 0 & 0 & 0 & 0 & 0 & 0 & 0 & 0 & 0 \\ 0 & 0 & 0 & 0 & -\Omega_N & 0 & 0 & 0 & 0 & 0 & 0 & 0 & 0 & 0 & 0 \\ 0 & 0 & 0 & 0 & 0 & 0 & 0 & \Omega_D & 0 & \Omega_D & 0 & 0 & 0 & 0 & 0 \\ 0 & 0 & 0 & 0 & 0 & 0 & -\Omega_D & 0 & \Omega_N & 0 & \Omega_D & 0 & 0 & 0 & 0 \\ 0 & 0 & 0 & 0 & 0 & 0 & 0 & -\Omega_N & 0 & 0 & 0 & \Omega_D & 0 & 0 & 0 \\ 0 & 0 & 0 & 0 & 0 & 0 & -\Omega_D & 0 & 0 & 0 & \Omega_D & 0 & \Omega_N & 0 & 0 \\ 0 & 0 & 0 & 0 & 0 & 0 & 0 & -\Omega_D & 0 & -\Omega_D & 0 & \Omega_N & 0 & \Omega_N & 0 \\ 0 & 0 & 0 & 0 & 0 & 0 & 0 & 0 & -\Omega_D & 0 & -\Omega_N & 0 & 0 & 0 & \Omega_N \\ 0 & 0 & 0 & 0 & 0 & 0 & 0 & 0 & 0 & -\Omega_N & 0 & 0 & 0 & \Omega_D & 0 \\ 0 & 0 & 0 & 0 & 0 & 0 & 0 & 0 & 0 & 0 & -\Omega_N & 0 & -\Omega_D & 0 & \Omega_N \\ 0 & 0 & 0 & 0 & 0 & 0 & 0 & 0 & 0 & 0 & 0 & -\Omega_N & 0 & -\Omega_N & 0 \end{bmatrix}$$

TABLE B-2 (Continued)

PARAMETERS USED IN FIGURE B-1

Ω – earth's angular rate

Ω_N – Ω cos (Lat)

Ω_D – $-\Omega$ sin (Lat)

g – gravity

P_g – axial mass unbalance drift rate compensation coefficient

R – radius of the earth

k_1, k_2 – vertical channel damping coefficients (see Appendix A)

$1/\beta_{VN}$, $1/\beta_{VE}$, $1/\beta_{VD}$ – correlation time of random accelerometer errors

$1/\beta_{\epsilon N}$, $1/\beta_{\epsilon E}$, $1/\beta_{\epsilon D}$ – correlation time of random drift rate errors

$$\underline{u}_x^L = \begin{bmatrix} u_{xN} \\ u_{xE} \\ u_{xD} \end{bmatrix}$$

$$\underline{u}_y^L = \begin{bmatrix} u_{yN} \\ u_{yE} \\ u_{yD} \end{bmatrix}$$

$$\underline{u}_z^L = \begin{bmatrix} u_{zN} \\ u_{zE} \\ u_{zD} \end{bmatrix}$$

} unit vectors along case-fixed X,Y,Z axes coordinatized in the L-frame

for those error sources which occur in the M-frame, the assumption of statistical independence was made relative to this frame. Consequently, there was considerable cross-correlation among the corresponding model states which were defined relative to the L-frame. Also, because many of the model states were products of an error source and a function of the MESG RSA direction vectors, it was necessary to construct the initial covariance matrix, P_0, from the program input parameters which described the error statistics and the RSA vectors.

To compute the L-frame covariance from the M-frame statistics requires a simple transformation using C_M^L, the coordinate transformation from the M-frame to the L-frame. For example, if $P_{\varepsilon B1}^M$ is the covariance matrix defining the three case-fixed bias terms of MESG No. 1 in the gyro (M) frame,

$$P_{\varepsilon B1}^M = \begin{bmatrix} \sigma^2_{\varepsilon B1_X} & 0 & 0 \\ 0 & \sigma^2_{\varepsilon B1_Y} & 0 \\ 0 & 0 & \sigma^2_{\varepsilon B1_Z} \end{bmatrix} \qquad \text{(B-2)}$$

then

$$P_{\varepsilon B1}^L = \begin{bmatrix} \sigma_{\varepsilon B1N} & \sigma_{\varepsilon B1N}\,\sigma_{\varepsilon B1E} & \sigma_{\varepsilon B1N}\,\sigma_{\varepsilon B1D} \\ \sigma_{\varepsilon B1N}\,\sigma_{\varepsilon B1E} & \sigma^2_{\varepsilon B1E} & \sigma_{\varepsilon B1E}\,\sigma_{\varepsilon B1D} \\ \sigma_{\varepsilon B1N}\,\sigma_{\varepsilon B1D} & \sigma_{\varepsilon B1E}\,\sigma_{\varepsilon B1D} & \sigma^2_{\varepsilon B1D} \end{bmatrix} \qquad \text{(B-3)}$$

can be computed as

$$P^{L}_{\varepsilon B1} = C^{L}_{M} \; P^{M}_{\varepsilon B1} \; C^{L}_{M}{}^{T} \qquad \text{(B-4)}$$

The process of constructing an initial covariance matrix corresponding to the state vector defined in Table B-1 from program input parameters is straightforward, but since it is rather tedious to enumerate, a detailed presentation will not be included in the appendix. With the definition of the system state vector and the system matrices F, Q and P, all the equations necessary for the covariance error analysis program have been presented.

APPENDIX C

REDUNDANT AXIS CONTROL IN THE MICRON MECHANIZATION

The purpose of this appendix is to demonstrate that the redundant axis control that appears in the MICRON mechanization equations (Ref. 14) maintains

$$\underline{S}_{N1} \cdot \underline{S}_{N2} = \underline{\gamma}_{c1} \cdot \underline{\gamma}_{c2} \qquad \text{(C-1)}$$

where $\underline{S}_{N1}$ and $\underline{S}_{N2}$ are the estimates of the RSA direction vector in the navigation frame coordinates and $\underline{\gamma}_{c1}$ and $\underline{\gamma}_{c2}$ are the compensated readouts of the RSA vectors (coordinatized in the M-frame). As was discussed in Chapter 3, it is important that Eq. (C-1) be valid because the inertial (S) frame in which the accelerometer outputs are integrated is not an orthogonal coordinate system. For this presentation, the updates to the spin vector estimates, $\underline{S}_{N1}$ and $\underline{S}_{N2}$, to incorporate the effects of vehicle motion, earth rate, and estimated drift rate are ignored since they are applied correctly to each direction cosine vector and are thus not an important part of the redundant axis control analysis.

Considering $\underline{S}_{N1}$ as the primary MESG, Fig. C-1 is a block diagram representation of the redundant axis control. Ignoring the sampled data aspects, since the 1/16 sec sampling rate should not introduce any significant error, it can be seen that

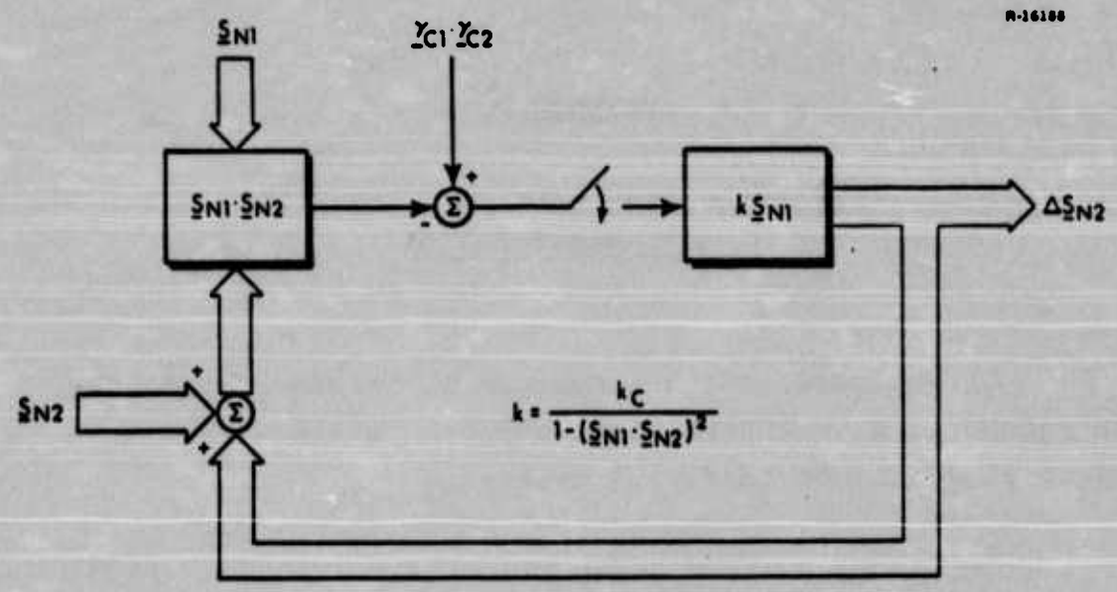

Figure C-1 Block Diagram of Redundant Axis Control (MESG No. 1 Primary)

$$\underline{S}_{N1} \cdot \underline{S}_{N2} = \underline{S}_{N1} \cdot \left(\underline{S}_{N2} + \Delta\underline{S}_{N2}\right)$$

$$= \underline{S}_{N1} \cdot \left(\underline{S}_{N2} + \frac{k}{1+k}\left(\underline{\gamma}_{c1} \cdot \underline{\gamma}_{c2} - \underline{S}_{N1} \cdot \underline{S}_{N2}\right)\underline{S}_{N1}\right)$$

$$= \underline{S}_{N1} \cdot \underline{S}_{N2} - \frac{k}{1+k}\left(\underline{S}_{N1} \cdot \underline{S}_{N2}\right) + \frac{k}{1+k}\left(\underline{\gamma}_{c1} \cdot \underline{\gamma}_{c2}\right)$$

(C-2)

Equation (C-2) can be seen to force $\underline{S}_{N1} \cdot \underline{S}_{N2}$ to track $\underline{\gamma}_{c1} \cdot \underline{\gamma}_{c2}$ which is the desired effect of redundant axis control. The MICRON mechanization has selected the gain

$$k = \frac{k_c}{1 - \left(\underline{S}_{N1} \cdot \underline{S}_{N2}\right)^2} \qquad \text{(C-3)}$$

The choice of gain in Eq. (C-3) increases the redundant axis control in a manner proportional to the nonorthogonality of $\underline{S}_{N1}$ and $\underline{S}_{N2}$. As the nonorthogonality increases, it is more critical that the estimated angle between the spin vectors ($\underline{S}_{N1} \cdot \underline{S}_{N2}$) track the measured angle ($\underline{\gamma}_{c1} \cdot \underline{\gamma}_{c2}$) to avoid introducing errors due to the use of the nonorthogonal inertial (S) coordinate frame in the MICRON mechanization.

REFERENCES

1. Bortz, J.E., Sr., "MICRON Analysis, Vol. I, MESGA Attitude Readout Error Model," The Analytic Sciences Corp., Report No. AFAL-TR-72-228, Vol. I, May 1972.

2. Bortz, J.E., Sr., "MICRON Analysis, Vol. II, MESGA Drift Model," The Analytic Sciences Corp., Report No. AFAL-TR-72-228, Vol. II, May 1972.

3. Blaschke, T.C. and Shields, J.D., "MICRON Analysis, Modeling, Calibration and Simulation," The Analytic Sciences Corp., Report No. AFAL-TR-73-374, March 1974.

4. Shields, J.D., "Micro-Navigator (MICRON) Analysis, Unified Calibration Development," The Analytic Sciences Corp., Report No. AFAL-TR-74-211, August 1974.

5. "Specification for the Micro-Navigator (MICRON) Interial Measurement Unit (IMU)," Air Force Contract No. F33615-74-C-1099, Statement of Work, 10 May 1974.

6. Ebert, W.A., "Micro-Navigator (MICRON) Phase 1A Final Report," Vols. 1-4, Autonetics Division of North American Rockwell, Report No. AFAL-TR-72-182, Vols. 1-4, July 1972.

7. Ebert, W.A., "Micro-Navigator (MICRON) Phase 1B Interim Report," Autonetics Division of North American Rockwell, Report No. C72-735.7/201, 11 December 1972.

8. Duncan, R.R., telephone conversation with J.D. Shields of TASC concerning Autonetics reduced preload studies, 8 March 1973.

9. D'Appolito, J.A., "The Evaluation of Kalman Filter Designs for Multisensor Integrated Navigation Systems," The Analytic Sciences Corp., Report No. AFAL-TR-70-271, January 1971.

10. Holmes, D.W. and Brasher, T.F., "Housing and Thermal Control, N57A Micro-Navigator (MICRON) System Detail Design Specification," Autonetics Division of North American Rockwell (no document number, undated).

REFERENCES (Continued)

11. Gelb, A., ed., Applied Optimal Estimation, MIT Press, 1974.

12. Nash, R.A., Jr., et al., "GEANS Error Minimization Study, Volume 1, Error Propagation Equations," The Analytic Sciences Corp., Report No. AFAL-TR-70-303, Vol. 1, 30 October 1970.

13. Mealy, G.L. and Shipp, R.F., "Sensor Data Bank Development; AN/ASN-90 Test Data File and Error Models," The Analytic Sciences Corp., Report No. AFAL-TR-74-233, August 1974.

14. Ebert, W.A., "Micro-Navigator (MICRON) Phase 1B Interim Report," Autonetics Division of North American Rockwell, Report No. C72-735.2/201, 11 August 1972.

15. Leondes, C.T., Ed., Guidance and Control of Aerospace Vehicles, McGraw-Hill Book Co., Inc., 1963.

16. Britting, K.R., Inertial Navigation Systems Analysis, Wiley-Interscience, 1971.

17. Jordan, S.K., "Self-Consistent Statistical Models for the Gravity Anomaly, Vertical Deflections, and Undulation of the Geoid," Journal of Geophysical Research, Vol. 77, No. 20, 10 July 1972.

18. Jordan, S.K., "Effects of Geodetic Uncertainties on a Damped Inertial Navigation System," IEEE Transactions on Aerospace and Electronic Systems, Vol. AES-9, No. 5, September 1973.

19. Broxmeyer, C., Inertial Navigation Systems, McGraw-Hill Book Co., Inc., 1964.

20. Ebert, W.A., "Micro-Navigator (MICRON) Phase 1B Test Plan," North American Rockwell Electronics Group, Report No. C72-806/201, September 1972.

21. Higley, R.B., et al., "Micro-Navigator (MICRON) Phase 1B Final Report for the Period 1 May 1972 through 27 November 1973, Vols. 1-3," Rockwell International, Report No. AFAF-TR-74-178, July 1974.

22. Bump, H.L., et al., "Micro-Navigator (MICRON) Phase 1B Letter Technical Progress Report," Autonetics Division of Rockwell International, Report No. C72-735.22/201, 18 February 1974.

23. "Slides for the MICRON Phase 1B Second Design Review - 8 and 9 January 1973," Autonetics Division of Rockwell International, 8 January 1973.

24. Bump, H.L., et al., "MICRON Fast Reaction and High Temperature Operation Development Final Report," Autonetics Division of Rockwell International, Report No. ECOM-0188-F, June 1974.

25. Miller, J.M., "Micro-Navigator (MICRON) Phase 2A Research and Development Status Report," Autonetics Group of Rockwell International, Report No. C74-455.3/201, 16 August 1974.

26. Nash, R.A., Jr., and Hutchinson, C.E., "Altitude Damping of Space Stable Inertial Navigation Systems," IEEE Transactions on Aerospace and Electronic Systems, Vol. AES-9, No. 1, January 1973.